applied sciences

MDPI

Article

Techno-Economic Potential of Plasma-Based CO_2 Splitting in Power-to-Liquid Plants

Samuel Jaro Kaufmann *, Paul Rößner, Stephan Renninger, Maike Lambarth, Moritz Raab, Jan Stein, Valentin Seithümmer and Kai Peter Birke

Electrical Energy Storage Systems, Institute for Photovoltaics, University of Stuttgart, Pfaffenwaldring 47, 70569 Stuttgart, Germany

* Correspondence: samuel.kaufmann@ipv.uni-stuttgart.de; Tel.: +49-711-685-67172

Abstract: Mitigating climate change requires the development of technologies that combine energy and transport sectors. One of them is the production of sustainable fuels from electricity and carbon dioxide (CO_2) via power-to-liquid (PtL) plants. As one option for splitting CO_2, plasma-based processes promise a high potential due to their flexibility, scalability, and theoretically high efficiencies. This work includes a modeling and techno-economic analysis. A crucial element is the process of the joint project PlasmaFuel, in which two plasma technologies are included in a PtL plant to produce synthetically sulfur-free marine diesel. The results are divided into three scenarios, which differ in the use of different boundary conditions and thus represent different degrees of technology development. The evaluation results in process efficiencies from 16.5% for scenario 2018/20 to 27.5% for scenario 2050, and net production costs between EUR 8.5/L and EUR 3.5/L. Furthermore, the techno-economic potential is mapped in order to open up development steps in the direction of costs below EUR 2.0/L. The present work allows statements regarding system integration and the industrial use of the plasma-based process.; moreover, conclusions can be drawn towards the most important levers in terms of process optimization.

Keywords: techno-economic analysis; reaction engineering; CO_2 conversion; dielectric barrier discharge; gliding arc discharge; plasma catalysis; sustainability; plasma processes; oxygen extraction

check for updates

Citation: Kaufmann, S.J.; Rößner, P.; Renninger, S.; Lambarth, M.; Raab, M.; Stein, J.; Seithümmer, V.; Birke, K.P. Techno-Economic Potential of Plasma-Based CO_2 Splitting in Power-to-Liquid Plants. *Appl. Sci.* **2023**, *13*, 4839. https://doi.org/10.3390/app13084839

Academic Editor: Luca Fiori

Received: 20 March 2023
Revised: 4 April 2023
Accepted: 6 April 2023
Published: 12 April 2023

Copyright: © 2023 by the authors. Licensee MDPI, Basel, Switzerland. This article is an open access article distributed under the terms and conditions of the Creative Commons Attribution (CC BY) license (https://creativecommons.org/licenses/by/4.0/).

1. Introduction

Mitigating climate change requires the development of technologies that combine energy and transport sectors. One of them is the production of sustainable fuels from electricity and carbon dioxide via power-to-liquid (PtL) processes. As one option of splitting CO_2, plasma-based processes promise a high potential due to their flexibility, scalability, and theoretically high efficiencies. The use of renewable energies to operate the traffic and transport sector plays an important role due to the high energy requirements and the large part of global CO_2 emissions (20%) [1].

Driven by economic and political interests, renewable energies are set to become the dominant source of electricity worldwide. Based on announced pledges by governments, the global share of electricity in total final energy consumption will rise from 20 percent in 2021 to 24 percent in 2030 and up to 39 percent in 2050 [2]. According to reports of the European government, the share of renewable energy in Europe has more than doubled between 2004 and 2021 [3].

In Germany, for example, the installed electrical capacity of renewable energies was expanded from 4.4 MW in 1990 to 139 GW (46% wind, 42% photovoltaics) in 2021 [4].

New acceleration plans were also published at the beginning of 2023 to further accelerate the expansion. One target is the expansion of offshore wind power plants from 8 GW (2022) to 30 GW (2030) and then to 70 GW (2045) [5].

The goal of the expansion of renewable energies is not only the conversion of the power supply but also the electrification of various sectors, especially the transport segment and

the chemical industry. In addition to accelerating the expansion of renewable energies, the German government published a power-to-liquid (PtL) roadmap in 2021 [6]. The roadmap defines measures to enable CO_2-neutral and sustainable flying. As the electrification of air traffic is hardly possible according to the current state of knowledge, this transport sector will have to rely on liquid fuels (hydrocarbons) in the long term. In the PtL roadmap, the annual use of 200,000 t of synthetic PtL kerosene is formulated as a target by 2030. This corresponds to approximately 2% of the kerosene refueled annually in Germany (as of 2019). The PtL roadmap identifies alternative syngas production as an important step toward achieving the defined targets.

The consumption share of syngas for the production of chemicals is around 80%. The demand for syngas is estimated to grow approximately 5% per year with a value of 4.21×10^{11} m^3 (normal cubic meters) in 2022, leading to high CO_2 emissions in conventional production. The main source of syngas production is coal, with a share of 50%, followed by natural gas at around 15%. Sixty percent of the production and half the consumption of syngas take place in China [7].

Since fossil fuels are finite and recent crises have shown us how quickly the price of natural gas can rise (500% percent price rise in Germany from mid–2021 to mid–2022 [8]), defossilization is a necessary step alongside electrification and decarbonization.

Due to the high demand for syngas and the desire for defossilization, the question of the best-performing PtL processes is huge. In addition to the further development of individual process steps, system integration and the interaction of individual process components take on an important role. Gas separation processes for coupling, in particular, play an important role in system integration. Economically, these process steps have had a major impact, which has been investigated, for example, in the study by Sofia et al. on the use of selective membranes for hydrogen [9]. For better planning and further development of PtL plants, process engineering modeling and coupled analyses are indispensable.

In the report "E-Fuels: a techno-economic assessment of European domestic production and imports towards 2050", published in 2022 by Concawe [10], individual power-to-liquid plants were considered techno-economically. Based on the boundary conditions, fuel costs for synthetic diesel were estimated between EUR 1.9/L and EUR 2.9/L for the year 2050, depending on the location in Europe (e.g., Germany: EUR 2.4/L). The location-dependent cost variation is due to the cost of electricity, which is expected to be higher in Northern and Central Europe than in Southern Europe. The cost of electricity consists of slightly above 60% of the costs. The considered power-to-liquid process uses hydrogen generated via electrolysis to thermo-chemically split CO_2 in a reverse water gas shift reaction (RWGS) at 800 to 1000 °C and 30 bar pressure. The efficiency of the RWGS reaction was assumed to be 83%. As an alternative to synthetic diesel, it is possible to produce other electricity-based fuels from syngas, such as methanol or dimethyl ether [11]. The results of the Concawe report show that these require lower manufacturing costs than synthetic diesel. Nevertheless, the prices will be at least twice as high as fossil diesel of EUR 0.8/L in 2050 [10].

In their paper from 2016, Albrecht et al. also showed techno-economic results for power-to-liquid plants with Fischer–Tropsch synthesis with an RWGS reaction for CO_2 splitting [12]. They obtain fuel costs between EUR 2.2 and EUR 2.8/L as a result, with a 60% share of electricity costs.

The research initiative Energiewende im Verkehr (EiV) of the German Ministry for Economy and Climate Protection (BMWK) deals with the use of electricity-based fuels. More than 100 research groups that deal with alternative fuels for large transport volumes and distances are being funded [13]. The results of the research groups should promote the coupling of the electricity and transport sectors and enable a reduction in greenhouse gas emissions. The individual joint projects are networked via the accompanying research on the energy transition in transport (BEniVer) of the German Aerospace Center (DLR). Its focus is on the consideration of technical, economic, ecological, and social effects. A standardized method for determining the production costs is being used to compare the individual fuel production processes.

The PlasmaFuel joint project (2018–2022) in EiV, which includes the Institute for Photovoltaics (*ipv*) at the University of Stuttgart, dealt with the plasma-induced production of fuel for shipping. In a PtL process using electricity from renewable energies, plasma-induced CO_2 splitting is linked to fuel production via the Fischer–Tropsch synthesis (FTS), as shown in Figure 1. In this project, the plasma-based splitting of CO_2 into carbon monoxide (CO) and oxygen (O_2) through a dielectric barrier discharge (DBD) and a variation of a gliding arc discharge (GA) was carried out. Through subsequent oxygen separation, the CO was synthesized together with electrolysis-H_2 in a Fischer–Tropsch reactor to form marine diesel. The energy required for this was supplied by excess wind power.

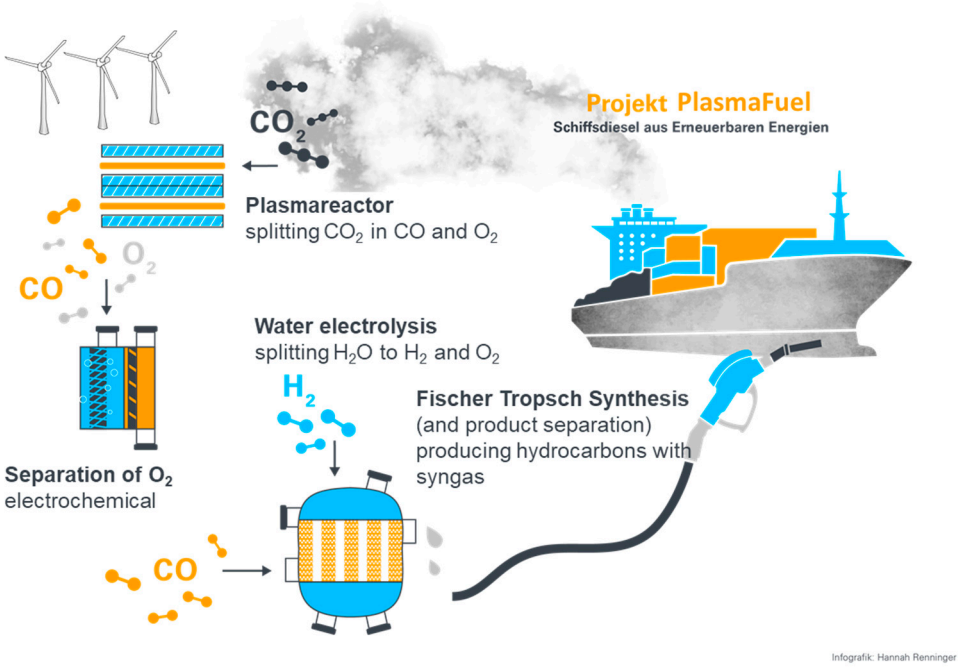

Figure 1. PlasmaFuel Project scheme (credit to Hannah Renninger).

The Smart Freight Centre and the European Chemical Industry Council provide average values of transport CO_2 emissions (g CO_2 per t km) for chemical–pharmaceutical industry transports [14]. The values for road transport are 71, for rail transport 19, for inland waterway ships 25, for ocean-going ships only about 4, and for airplanes 1060 g_{CO2}/tkm. Due to very high loading capacities and comparatively low CO_2 emissions, large-scale transports by container ship cannot be replaced.

The generation of electricity-based marine diesel is an important area of development for several reasons. On the one hand, the electrification of shipping is not feasible. The reasons for this are the high costs and excessive mass of the battery units needed, based on their low energy densities and the charging infrastructure. In the following case example, the problem is taken up again. The energy consumption of a big container ship with a typical 200.000 t payload over a 10.000 km transport distance ($\approx 8 \times 10^6$ kg CO_2) can be estimated as bigger than 10^{13} J (dimensions: 400 m, 60 m, 15 m; a cruising speed of 10 m/s, and friction value of 0.0025). Comparing the specific energy of chemical fuels ($\sim 10,000$ Wh/kg) and electrochemical cells (~ 300 Wh/kg), much of the payload must be dispensed. With a usual 1 day of charging, the ship would need more than 300 MW of electrical power to fill the energy storage. On the other hand, conventional ship fuel releases sulfur emissions when burned; to reduce these emissions, the shipping industry is striving to further develop exhaust gas cleaning systems and to use alternative fuels. An alternative to synthetic fuel is the use of hydrogen and conversion to electricity in fuel cells. Since the storage of gaseous hydrogen under high pressure involves very large reservoirs

due to the low density, and liquefaction requires very costly insulation and energy for cooling, integration in long-haul aircraft and container ships is still problematic.

In summary, it can be said that the production of synthetic fuels for the ship and aviation sectors is an important part of the energy transition. The development and optimization of technologies such as CO_2 splitting are necessary to design the required power-to-liquid plants. In addition, considerations of the entire process chain and investigation and comparison of technical and economic performances are necessary. This can be carried out through techno-economic analyses, in which the costs of a fuel produced can be estimated.

In addition to previous studies on the feasibility of synthetic fuels, this work provides insights into the integration of plasma-based CO_2 splitting into PtL plants. The work, thus, extends the previously considered paths to synthetic fuels by a plasma-based option. For this purpose, the reactors investigated in the PlasmaFuel joint project are integrated into a process chain to produce sulfur-free sustainable marine diesel. Since processes of plasma-based CO_2 splitting have several advantages but still require further development, this work examines its feasibility and economic potential. The modeling and techno-economic analyses address the research questions: How expensive is the production of plasma-induced, pollution-free sustainable fuels? What are the biggest levers regarding efficiency? Is it possible to produce plasma-based synthetic diesel for EUR 2.0/L or less? How big is the impact of the electricity costs via renewable energies?

2. State of the Art

In the following, a brief review of plasma-based CO_2 splitting is presented. In the reviewed literature, no techno-economic consideration of system integration in PtL plants has been considered so far; therefore, this work provides a valuable addition to the consideration of this plasma application.

2.1. Plasma-Based CO_2 Splitting—A Short Review

Plasma technologies are promising in power-to-liquid processes due to their simple operating conditions and flexible use as renewable electrical energy. The term plasma describes an ionized gas in which at least one electron is not bound. Plasma can be achieved from the gaseous third state of matter by heat input, electric fields, and radiation. In non-thermal plasma, the temperatures of the individual plasma parts differ significantly. The electron temperature of about 10,000 K is significantly higher than all other temperatures (neutral particles, oscillating particles, ions). As a result, reactions operate in non-thermal plasmas that could not occur from a thermal point of view. Warm plasma represents a middle ground between thermal and non-thermal plasma. It contains properties of both types of plasma and is characterized by both high electron density and a high degree of non-equilibrium. Bogaerts and Centi describe this type of plasma as very promising for CO_2 conversion due to its high process flexibility, which allows different types of reactions to be carried out (e.g., pure CO_2 splitting, as well as CO_2 conversion in the presence of CH_4, H_2, or H_2O [15–17]).

In addition, the investment and operating costs are very low, and rare earth metal-based catalysts are not necessarily required for the reactions. Another advantage is its possible application in a modular environment, since plasma reactors are linearly scaled with the plant capacity, allowing production according to demand. One of the most important advantages is the very simple linkage with renewable electricity. When plasma generation is combined with an additionally introduced catalyst, this is referred to as plasma catalysis. A distinction is made between in-plasma catalysis (catalyst in the plasma) and post-plasma catalysis (catalyst after the plasma). Compared to thermal processes, significantly smaller amounts of catalysts are required, and reactions can be carried out at much milder operating conditions (low pressures, low temperatures) due to the properties of non-thermal plasmas. In addition, interactions occur between the plasma and the catalyst (e.g., changes in the electric field or changes in the catalyst surface), which positively affects

both. The applications of plasma catalysis are versatile, and Table 1 shows some processes, their reactants, and products, as well as their technology readiness levels (TRL) [15].

Table 1. Applications of plasma catalysis and their technology readiness levels (TRL) in accordance with [15]. (VOC = volatile organic compounds).

Process	Educts	Products	TRL
CO_2 splitting	CO_2	CO, O_2	2–3 [18]
CO_2 splitting	CO_2, CH_4	CO, H_2	2–4 [19]
CO_2 splitting	CO_2, H_2O	CO, H_2	1–2 [18]
CH_4 splitting	CH_4	H_2	2–4 [20]
Air purification	VOC	CO_2, H_2O	6–7 [21]
Odor control	Odors/air	Harness connections	8–9 [22]
NH_3 synthesis	N_2, H_2	NH_3	1–2 [23]
Tar reforming	Tar	CO, H_2	2–3 [24]
Methanol splitting	MeOH, H_2O	H_2	1–2 [25]

The challenges in applying plasma catalysis are the optimization and control of processes in terms of conversion, selectivity, and efficiency. Since the vibrational excitations triggered in the plasma significantly reduce the activation energy of reactions, plasma-based processes and plasma catalysis have very high potential in terms of energy efficiency. Moreover, the interactions between plasma and the catalyst are still not clear due to their complexity and require real-time studies directly at the interaction sites. In addition to a better understanding of plasma–catalyst interactions, Tu et al. mentioned the further engineering development of plasma processes regarding new reactor designs and further process engineering adaptations as an important step toward the optimal exploitation of this potential [26].

To compare different plasma processes in the field of CO_2 splitting—conversion and efficiency must be considered. The efficiency η_{CO_2} of the plasma-based CO_2 splitting can be assumed to consist of the effective conversion of CO_2 χ_{CO_2}, and the specific energy input SEI is related to the standard reaction enthalpy of the CO_2 splitting reaction of $\Delta H^{298.15K} = 283 \frac{\text{kJ}}{\text{mol}}$ [18].

$$\eta_{CO_2} = \frac{\chi_{eff} \cdot \Delta H^{298.15K}}{SEI} \tag{1}$$

$$\chi_{eff} = \chi_{CO_2} \cdot \frac{\dot{n}_{CO_2 in}}{\dot{n}_{in}} = \frac{\dot{n}_{CO_2 in} - \dot{n}_{CO_2 out}}{\dot{n}_{CO_2 in}} \tag{2}$$

$$SEI = P_e / \dot{n}_{CO_2,in} \tag{3}$$

where $\dot{n}_{CO_2,in}$ is the molar stream of CO_2 at the inlet of the reactor, $\dot{n}_{in}$ is the molar stream at the inlet of the reactor, $\dot{n}_{CO_2,out}$ is the molar stream of CO_2 at the outlet of the reactor, and P_e is the electric power input to the reactor.

Snoeckx and Bogaerts et al. considered the different plasma technologies for CO_2 splitting in their 2017 study [18]. The paper focused on dielectric barrier discharge, and gliding arc and microwave plasmas. Different studies were summarized and plotted in a conversion–efficiency diagram. Microwave plasmas with both a high conversion and efficiency stood out. Gliding arc plasmas achieve high efficiencies with low conversions. Dielectric barrier discharge (DBD) plasmas perform worse due to the reduced field strength deviating from Microwave plasma (MW) and gliding arc plasma (GA), with a few exceptions.

In a comparative study from 2021 by Renninger et al., experimental studies on plasma-based CO_2 splitting were considered and compiled [27]. Only studies that achieved comparatively high conversions and/or efficiencies for the individual technologies were included. Minor extensions were made to the original diagram; the adjusted diagram is shown in Figure 2.

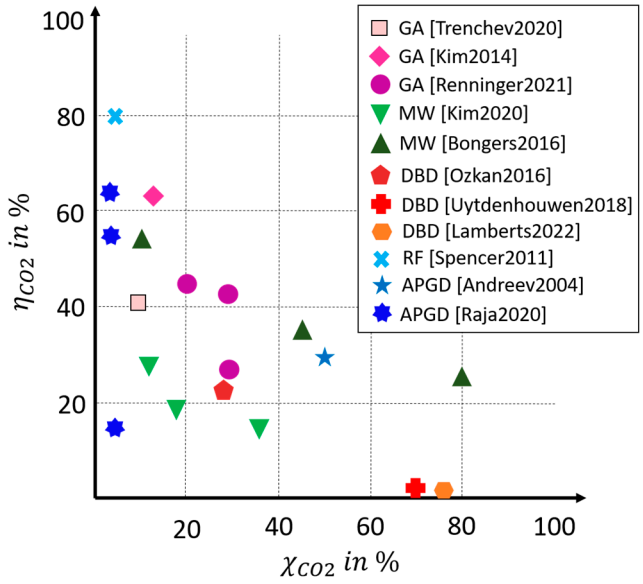

Figure 2. Experimental conversion rates χ_{CO_2} and energy efficiencies η_{CO2} of plasma technologies for CO_2 conversion [Renninger2021] [27]: gliding arc discharge (GA) performed by Trenchev et al. [Trenchev2020] [28], Kim et al. [Kim2014] [29] and Renninger et al. [Renninger2021] [27]. Microwave plasma (MW) was performed by Kim et al. [Kim2020] [30] and Bongers et al. [Bongers2016] [31]. Dielectric barrier discharge (DBD) was performed by Ozkan et al. [Ozkan 2016] [32], Uytdenhouwen et al. [Uytdenhouwen2018] [33], and Lamberts et al. [Lamberts2022] [34]. Radio frequency discharge (RF) was performed by Spencer et al. [Spencer2011] [35]. Atmospheric glow discharge plasma (APGD) was performed by Andreev et al. [Andreev2004] [36] and Raja et al. [Raja2020] [37].

Ozkan et al. conducted experiments with a coaxial DBD reactor, varying a number of parameters, including the flow rate, operating frequency, power, barrier thickness, and duty cycle [38]. By using a burst mode, they were able to achieve an efficiency of 23%, which is comparably high for a DBD reactor, with a conversion of 26%. Uytdenhouwen et al. achieved the highest DBD conversions of 71% by reducing the gap size of the reactor; however, the efficiency of the reactor was only 2.5% [39].

Lamberts et al. published a techno-economic assessment of CO_2 splitting with a DBD reactor in 2022. Experiments were carried out on a coaxial design with an integrated catalyst-packed bed [34]. The packed bed, the residence time, the specific energy input, and the feed were varied. When varying the feed, pure CO_2 splitting and dry reforming of methane (CO_2 and CH_4 feed) were investigated. For the analysis of the economic feasibility, the net present value (NPV) was determined, which offset incoming and outgoing cash flows. This resulted in only negative values that were largely due to the high electricity costs, which were assumed to be EUR 80/MWh in the study. Among the considered experiments, the studies with CO_2 and CH_4 performed better than the pure CO_2 splitting. For CO_2 splitting, a maximum conversion of $\chi_{CO_2} \approx 75\%$ with an $SEI = 3.5 \times 10^8$ J/kg$_{CO_2}$ ($P = 30$ W, $\dot{V} = 2.6 \times 10^{-3}$ SLM) was achieved. The energetic consideration was carried out via the specific energy consumption, which amounted to 90 MJ/mol at the maximum conversion. Converted into the previously defined efficiency of CO_2 splitting, this resulted in $\eta_{CO_2} = 0.31\%$. At $SEI = 6.2 \times 10^7$ J/kg$_{CO_2}$, a conversion of 40% was obtained with a specific energy consumption of 30 MJ/mol ($\eta_{CO_2} = 0.94\%$). Under the mixture of CH_4 (ratio 1:1 molar), conversions of $\chi_{CO_2} \approx 85\%$ were obtained with a specific energy consumption of 80 MJ/mol. In the economic analysis, capital costs of $CAPEX =$ EUR 188,143 were estimated for a 144 kW pilot plant, based on reactor costs and the associated power supply, which corresponds to specific costs of EUR 1.300/kW for this size.

As part of the PlasmaFuel joint project, a gliding arc reactor was developed, and its results were published in two papers by Renninger et al. [40,41]. The GA discharge plasma

reactor achieved a conversion of CO_2 of 27% at an energy efficiency of 42% at ambient pressure. The good performance was attributed to an efficient sweeping of the gas by discharge due to the magnetic field. The reactor setup used a magnetic field to force the plasma into a large disc-like volume and lead the working gas with a laminar gas flow through. The highest performance was achieved at $P_{el} = 160$ W and $\dot{V}_{in} = 1.25$ SLM, which corresponded to 3.89×10^6 J/kg_{CO_2}.

2.2. Oxygen Separation—Review and Experimental

Reducing carbon dioxide yields oxygen-rich gas, from which the oxygen must be extracted before further use is possible to inhibit recombination.

The amount of oxygen in the process gas was investigated in the PlasmaFuel project, and a 1% to 2% concentration was set as a maximum value that can be processed by the downstream Fischer-Tropsch synthesis. The influence of the oxygen content was investigated by Jess et al. [42]. To reduce the oxygen content to 1%, a variety of technologies can be applied. Commonly, adsorption technologies or nanoporous membranes are used; however, both are not able to deliver high-purity gases or extract traces of oxygen from gases. A lot of research is currently being undertaken on high-temperature solid electrolyte ion pumps, which offer high selectivity for oxygen. However, these systems require a catalyst as well, which can lead to coking issues when carbon monoxide is present. Finding high-temperature solutions that offer high current density while being robust is an ongoing field of research. Low-temperature electrolysis can resolve this issue in theory; however, a fitting catalyst is also required that is stable in the presence of carbon-containing gases.

Different oxygen separation approaches are characterized in the following. The challenge of oxygen separation lies in the gas composition of the mixed gas from which the oxygen is to be separated. Originally, a zirconium dioxide electrode was considered for this task. Commercially available zirconium dioxide membranes use a catalyst to split the molecular oxygen into atomic oxygen, which can be conducted. This is typically a platinum-group metal. Such catalysts are poisoned by carbon monoxide (CO) and carbon dioxide (CO_2), i.e., their active surface area decreases rapidly. Research reveals several potential alternative technologies. These include nanoporous membranes, which enable low-temperature applications. They are operated by diffusion, i.e., a pressure difference. The main disadvantage is their low separation efficiency due to the similar permeability of O_2, CO, and CO_2 of the membrane.

Better separation efficiencies are achieved by electrochemical methods. For example, a zirconium dioxide membrane has high selectivity and is commercially available but requires a working temperature $T > 600$ °C. Working temperature, selectivity, and flow rate are, therefore, relevant parameters. Perovskite membranes belong to the group of mixed ionic electric conductors (MIEC) and can be manufactured both monolithically and asymmetrically [43]. At low temperatures of $T = 150$ °C, they can be used as a catalyst for oxygen uptake. For significantly higher temperatures, the function of a separation membrane is also possible, although the asymmetric membrane has, so far, only been CO_2-resistant to a limited extent. In addition, a perovskite membrane is conceivable as an electrode for electrochemical substance separation, but developments of this kind would have to be pursued in cooperation with research groups experienced in this field.

Gas diffusion electrodes are another option and are used in the chemical industry. They achieve sufficient fluxes at low operating temperatures and sufficient selectivity. The question of a suitable catalyst also arises here. Pressure swing adsorption or temperature swing adsorption can both be used to separate oxygen from the gas mixture but require a large amount of energy in the form of heat [44]. The last technology considered is the molten carbonate fuel cell (MCFC) membrane, which can be used in reverse mode for oxygen separation. Currently, this patented membrane is only sold by one company at a very high price and is consequently not commercially available in a cost-efficient way.

The possible processes for oxygen removal are summarized graphically in Figure 3.

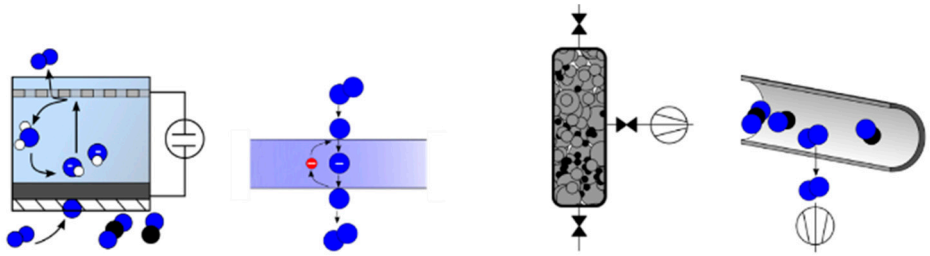

Figure 3. Possible processes for oxygen separation: electrochemically, mixed ionic electric conductor, adsorption, and diffusion.

After evaluating the possible technologies for extracting oxygen from a mixed gas stream, a separation process for PlasmaFuel has been selected. Because of its innovation potential and technical advantages, the gas diffusion electrode (GDE) was investigated.

Gas diffusion electrodes (GDE) are used in the fuel cell industry. As a multi-layer porous electrode made of active material and a hydrophobic layer, it enables the separation of oxygen (O_2) from a material flow. A mixed gas of CO_2, CO, and O_2, in which the O_2 is to be removed, is used as an example. The working principle and design of a GDE separation device is depicted in Figures 4 and 5, respectively. Oxygen gets into the adjacent electrolyte through the multi-layered GDE (cathode). The hydrophobic separator on the gas side ensures that no liquid electrolyte can penetrate the gas system. The active material of the GDE consists of a catalyst (e.g., silver oxide, manganese oxide) with graphite. The graphite gives the electrode sufficient porosity to allow gas and electrolyte to penetrate. The electrolyte used was 17% potassium carbonate solution (K_2CO_3).

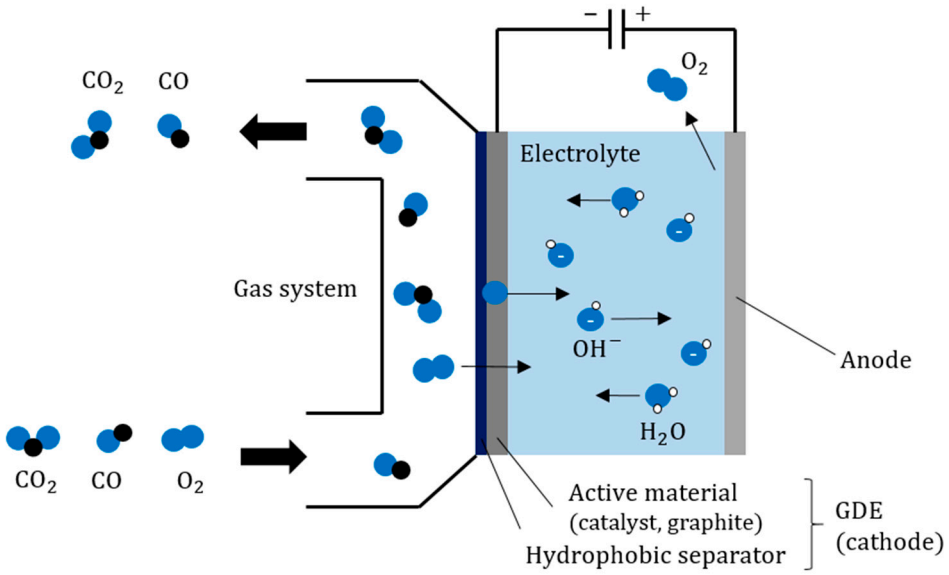

Figure 4. Scheme of the working principle of a gas diffusion electrode as an oxygen removal device.

The gas diffusion electrode currently under investigation uses graphite as the support and manganese dioxide (MnO_2) as the catalyst for oxygen reduction catalyst. MnO_2 is a weak catalyst commonly used in air-fed batteries. It is an electrochemical separation process of oxygen (O_2) from a mixed gas stream of predominantly carbon dioxide (CO_2) and carbon monoxide (CO), and the catalyst used is selective for the reduction of O_2. Oxygen is transported through the electrolyte in the form of OH^- ions. Due to the high conductivity of aqueous electrolytes, the system can achieve high current densities at low temperatures ($T < 90$ °C). By using a carbonate-based alkaline electrolyte, side reactions with the electrolyte are mitigated. Using a hydroxide-based electrolyte might work better initially, but they will quickly react to carbonates in situ.

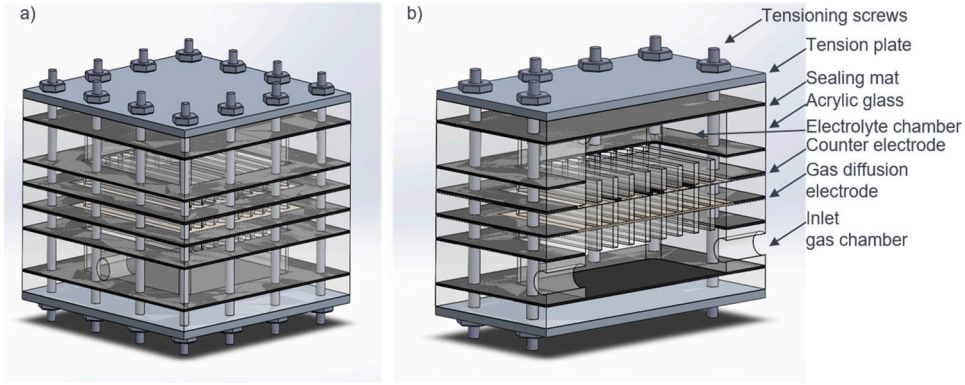

Figure 5. Technical design of a gas diffusion electrode device for the removal of oxygen. (**a**) Full construction. (**b**) Sectional view to show the layers as well as inlets and outlets.

The power needed to separate oxygen through the GDE is defined through:

$$P_{GDE} = U_{GDE} \cdot I_{GDE} = U_{GDE} \cdot \dot{n}_{O2} \cdot F \cdot z \quad (4)$$

According to the reaction equation at the GDE surface

$$\frac{1}{2}O_2 + H_2O + 2e^- \rightarrow 4OH^- \quad (5)$$

$z = 2$ is fixed.

A current density of $i = 18\ mA/cm^2$ was achieved with N_2/O_2 mixtures. When CO-rich gas from the plasma reactor was used, the current density dropped to 65% of the initial value before stabilizing. The operation was demonstrated successfully for a period of 10 h. The obtained results suggest that a higher current density could be achieved using a modified catalyst since the oxygen reduction and gas formation produce the highest potential.

3. Methodology

3.1. Goal and Benefit

Both the advantages and optimization needs of plasma-based CO_2 splitting were mentioned in the last chapter. Since previous studies on PTL plants with Fischer–Tropsch synthesis (FTS) have only considered a path with the reverse water gas shift (RWGS) from a techno-economic point of view, the model in this work presented and its results offer insights into the integration of plasma-based CO_2 splitting as a possible CO source for synthesis gas. To obtain the necessary high temperatures in the RWGS, gas combustion is necessary, which is acheived by adding natural gas or destroying a part of the product produced. This is not necessary when using plasma technologies and is an advantage in the direction of defossilization. A first techno-economic classification of DBD plasma has already been performed by Lamberts et al., but only for the experimental results obtained in the paper, which achieved high conversions but low efficiencies [34].

Another important point is the interaction with other PTL components, especially the necessary oxygen separation. Three different scenarios, 2018/20, 2030, and 2050, which differed in the use of different boundary conditions and thus represented different degrees of technology development, were considered, and further increases in efficiency, etc., are discussed. One advantage of the developed MATLAB model is the possibility of extending individual components and, thus, increasing the level of detail of certain model parts. By integrating characteristic diagrams from previous experiments, finer control levers can be addressed, and the influences on a possible overall system can be discovered at an early stage. It must be kept in mind that, in summary the optimization of small levers can also result in considerable increases.

3.2. Modelling

The process was modeled and techno-economically analyzed in MATLAB Simulink. An earlier version was modeled in ASPEN plus and techno-economically analyzed via TEPET (Techno-Economical Evaluation Tool), a tool of the DLR-Stuttgart. The older version was used to validate the new model. The core of the modeling was the PlasmaFuel process. A simplified block flow sheet is shown in Figure 6. A more detailed flowsheet is attached in Appendix A. The calculation in the model was carried out with steam tables of water, and the NASA-polynomial and Peng–Robinson equations.

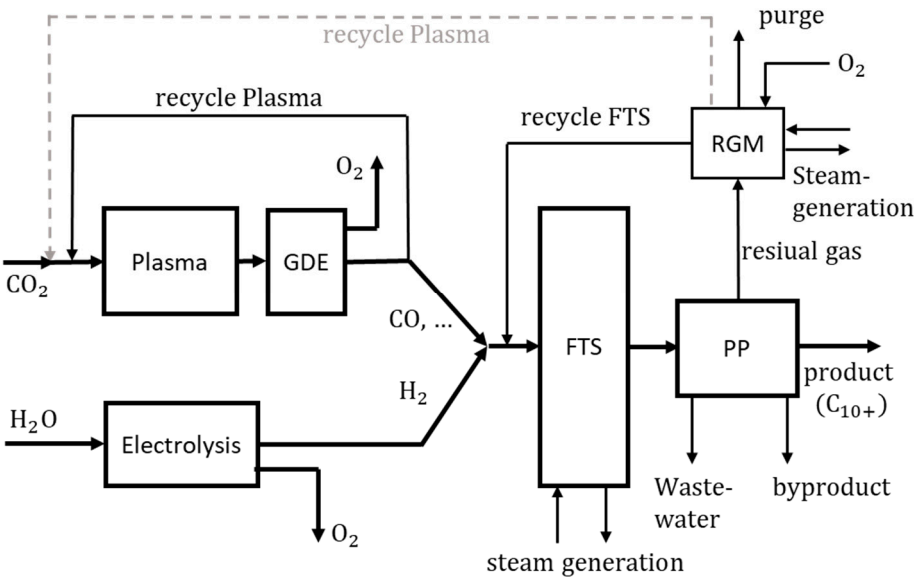

Figure 6. Block flowsheet of the modeled process consisting of the plasma-reactor, gas diffusion electrode (GDE), electrolysis, Fischer–Tropsch synthesis reactor (FTS), product preparation (PP), and residual gas management (RGM).

3.2.1. Electrolysis

In the model, an electrolysis system identical to alkaline electrolysis is depicted. It was a pressure electrolysis in which the pressure of $p = 30$ bar was applied upstream of the system by a pump. The efficiency of electrolysis is related to the lower heating value of hydrogen and was assumed to be calculated according to Formula (6) using efficiencies presented in the outlook of an IEA study [45]:

$$\eta_{EL} = \frac{\dot{n}_{EL,in} \cdot LHV_{H_2}}{P_{EL,e}} \quad (6)$$

3.2.2. Plasma-Based CO_2 Splitting

The plasma reactors operate at ambient pressure, and ambient temperature was present at the inlet. Depending on the plasma technology, the gas temperature across the reactor increased to 80 °C (DBD) or 400 °C (GA), as shown by experimental investigation. The electrical power P_{Plasma} needed to split the CO_2 was calculated using Formulas (1)–(3), under the use of η_{CO_2} and χ_{CO_2} as parameters.

3.2.3. Gas Diffusion Electrode

In the model, the necessary power P_{GDE} to extract the oxygen after CO_2 splitting was calculated through the formula in (4). Because P_{GDE} is not meant for determining equipment costs in GDE because of the changing current density while reducing the oxygen concentration x_{O_2}, the GDE area must be calculated, which is necessary to separate the desired amount of oxygen. For the determination of A_{GDE}, a characterizing size of the GDE was defined, the $A_{GDE,spec}$, which describes the GDE area per standard liter per

minute [SLM = 1 L/min]. It is a function of the current density curve iC_{GDE} as well as the concentrations x_{GDE,in,O_2} and x_{GDE,out,O_2}. To determine the specific area of the GDE, iterative calculations were carried out, in which small GDE elements were considered and combined to form an area. The calculations were integrated into the simulation block via a map. For the creation of the map, measurements were performed on the GDE. A container filled with air was connected to the GDE and oxygen was separated by varying the temperature T_{GDE} and voltage U_{GDE}. Under ambient pressure $p = 1$ bar, curves of the current density above the partial pressure of O_2 were obtained. The determination of $A_{GDE,spec}$ was found in MATLAB. Figure 7a shows a fit function of the measure performed in the lab at T = 80 °C and $U = 1.1$ V. The map resulting from the current density diagram is also shown in Figure 7b.

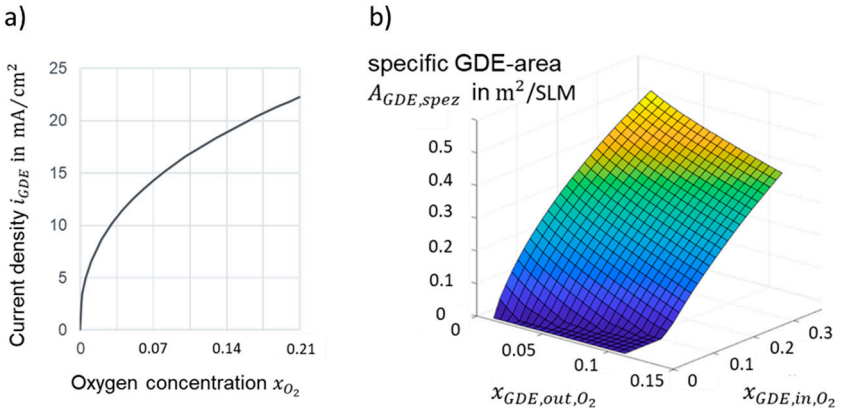

Figure 7. GDE modeling: (**a**) current density curve (fit function to experimental data), (**b**) map of specific GDE-area.

3.2.4. Fischer–Tropsch Synthesis

For fuel synthesis, a low-temperature Fischer–Tropsch synthesis (FTS) was modeled, which operated at 250 °C and 25 bar in a fixed-bed reactor with a cobalt catalyst. Based on the Anderson–Schulz–Flory (ASF) distribution, the mass fractions of the hydrocarbons at the outlet of the reactor are determined via [46]:

$$w_{Cn} = (1 - \alpha)^2 \cdot \alpha^{n-1} \cdot n \tag{7}$$

Since as many long-chain CH as possible are required for marine diesel, a chain growth probability of $\alpha = 0.9$ was selected. Research colleagues from Bayreuth reproduced this in their reactor. The mass fractions of long-chain waxes from C_{36+} were considered collectively. Since the methane selectivity was significantly higher than that of the ASF distribution, this was selected as a separate parameter, set to 14% as a boundary condition, and all other mass fractions were corrected on this basis. The fixed-bed reactor cooling is modeled by a cooling water flow used for steam generation. Technical limits for the FTS that were considered in the model were less than 50% inert gas at the input, as well as an oxygen concentration with a maximum of 1%, both that the reactor stays thermic stabile. The first was given through all simulation variations and second was one of the design-spec. parameters.

3.2.5. Other Model Components

Various pumps, compressors, and heat exchangers were integrated into the model. Since plasma-based CO_2 splitting takes place under ambient conditions, a water-cooled multistage compressor is required downstream, for example. The compressor capacity calculation was based on isentropic and polytropic state formulas, which included an isentropic efficiency. To determine the capital costs of the heat exchangers used, the heat transfer and the necessary surface area were determined from the flows, the heat

to be transferred, and the existing aggregate states. A recuperative heat exchanger was installed upstream of the Fischer–Tropsch synthesis, which preheated the synthesis gas and cooled the FTS product for product preparation. The product preparation consisted of various reactors, heat exchangers, and columns. Wastewater produced in the FTS and the gaseous products and unreacted synthesis gas were separated; this and the separation of the liquid hydrocarbons into main and by-products took place under different pressure and temperature levels. The separated gas phase then went further into the residual gas management. In this part of the model, the gases were partially fed into the recirculation and recompressed before the FTS, the remaining gas had to be purged for mass balance. For this purpose, the materials were burned to release CO_2, H_2O, and heat. A compressor and a turbine were integrated for energy recovery. There were recycle streams integrated into the model; one to achieve non-converted synthesis gas back in the FTS reactor for a larger amount of product, and one around the plasma reactor to increase the CO concentration in the synthesis gas.

3.2.6. Model Regulations

The model was controlled by separate regulation blocks—the following variables were regulated in these. The water input to the model was controlled by the specification of the total electrical power of the process P_{tot}. The required CO or CO_2 demand was controlled by a desired ratio:

$$r_{H_2CO} = n_{H_2,syngas} / n_{CO,syngas} \tag{8}$$

The ratio is set to a typical value for the FTS reactor of $r_{H_2CO} = 2$ before FTS synthesis. Another variable that is controlled is the oxygen capture in the GDE, which was controlled to the concentration limit of 1% O_2 at the FTS inlet. Furthermore, various cooling water and steam flows of the individual components were adjusted via control blocks and interconnected in a separate heat integration so that external heat requirements were no longer necessary.

3.3. Methodology of Techno-Economic Analysis

The technical evaluation of the overall process was carried out via the process efficiency:

$$\eta_{PTL} = \frac{\dot{m}_{product} \cdot LHV_{product}}{P_{e,tot}} \tag{9}$$

This relates the mass of the product produced together with its lower heating value to the total electrical power input:

$$P_{e,tot} = P_{Plasma} + P_{EL} + P_{GDE} + \sum P_{pump} + \sum P_c + \sum P_t \tag{10}$$

P_{Plasma}: Power of plasma-based CO_2 splitting;
P_{EL}: Power of electrolysis system;
P_{GDE}: Power of gas diffusion electrode;
P_{pump}: Power of water pump;
P_c: Power of a compressor;
P_t: Power of a turbine.

The techno-economic analysis focused on the calculation of the fuel costs incurred. The calculation methodology presented by Albrecht et al. was applied in a modified form [12]. Using the technically proven components represented in the industry, a deviation of $+/-30\%$ can be assumed for this type of cost estimation. Due to the inclusion of new components, such as the plasma reactor and the GDE, further deviations are to be expected. However, it is sufficient for a first estimation. In the process, equipment costs were first calculated using variables that arose in the individual components, which led to the capital costs $CAPEX$ via various factors. In addition to $CAPEX$, operating costs $OPEX$ were

determined, which were divided into indirect and direct costs. In addition, labor costs were determined. The equipment costs:

$$EC_i = CF_i \cdot \left(\frac{CEPCI}{CEPCI_{ref}} \right) \cdot F_{mat} \cdot F_{press} \tag{11}$$

Consist of the cost functions CF_i, which determines the cost dimension of the device from technical quantities, the chemical engineering plant cost index ($CEPCI$), which includes the time of the determination of the cost function, and factors due to higher requirements regarding material and pressure. After that, the fixed capital investment for each component was calculated through:

$$FCI_i = EC_i \cdot \left(1 + \sum_{j=1}^{10} F_j\right) \cdot \left(1 + \sum_{j=11}^{12} F_j\right) \tag{12}$$

Considering additional costs represented as factors F_j, these additional costs incurred were divided by Albrecht et al. into twelve areas or relationship factors. F_1 considers installation costs, F_2 instrumentation costs, F_3 necessary piping, F_4 electrical to be installed, F_5 building costs, F_6 site improvements, and F_7 installed service facilities. Factors F_8, F_9, and F_{10} consider indirect plant costs such as engineering, supervision, construction costs, and legal fees. F_{11} and F_{12} consider contractor fees and contingencies, and random events [12]. For the whole capital expenditure, a capital factor of 0.9 was used. For amortization of the $CAPEX$, over a plant lifetime y in years, the annual capital costs ACC are calculated with the annuity factor AF and the interest rate IR.

$$CAPEX = \frac{\sum FCI_i}{0.9} \tag{13}$$

$$ACC = CAPEX \cdot (0.9 \cdot AF + 0.1 \cdot IR) \tag{14}$$

$$AAF = (1 + IR)^y \cdot \frac{IR}{(1 + IR)^y - 1} \tag{15}$$

In addition to capital costs, operating costs also play a role in the production costs of fuels. These operational expenditures ($OPEX$) can be divided into direct and indirect costs. Direct operating costs

$$OPEX_{dir} = \sum \dot{m}_i \cdot c_i + \sum P_j \cdot c_e + \sum \dot{Q}_i \cdot c_Q \tag{16}$$

include costs through expenses and revenues and refer to specific market prices c_i. Direct operating costs thus refer to raw materials required, and by-products produced $\dot{m}_i$ (c_i), as well as outputs P_j (c_e) and heat flows $\dot{Q}$ (c_Q). In our model, no heat flows were drawn externally due to heat integration, so this term was omitted.

Indirect operating costs $OPEX$ include accruing maintenance costs, operating material costs, and laboratory fees. They were calculated using $CAPEX$ and the annual labor costs (ALC).

Finally, net production costs

$$NPC = \frac{ACC + OPEX_{dir} + OPEX_{ind} + ALC}{\dot{m}_{product} \cdot t} \tag{17}$$

summarizes all costs incurred and relates them to the annual mass production of the desired product for an annual operating time t.

3.4. Boundary Conditions

For the modeling and techno-economic analysis, different boundary conditions were assumed. Some of the parameters are varied within the chosen scenarios and sensitivity analyses. In Table 2, general plant parameters are shown first. These were selected in the PlasmaFuel joint project in consultation with BEniVer and were also included in the current model.

Table 2. Plant parameters.

Plant Parameter	Value
Electric power input	300 MW
Plant location	Germany
Plant lifetime	20 years
load	8000 h/year
Interest rate	5%
Labor cost	EUR 41/h
workforce	2 + 4/2 (300 MW), 1/3 (3 MW)

In Table 3, important technical parameters are listed, which were chosen in the modeling. In some cases, technical parameters were varied. This was due to the differentiation of various scenarios. The current state of the art is represented by the 2018/20 scenario, and the 2030 and 2050 scenarios were defined for an outlook. Assumptions were made for the outlook of the performance of the dielectric barrier discharge (DBD) and gliding arc (GA) plasma technologies. Information on temperature and pressure levels has already been given in the modeling text sections, so the table values are mainly about efficiencies.

Table 3. Important technical parameters of the modeled components.

Component	Parameter	Value	Reference
Electrolysis	efficiency	75% (S2018/20), 80% (S2030) 90% (S2050)	[45]
DBD-plasma-reactor	CO_2 conversion	26% (S2018/20), 30% (S2030) 40% (S2050)	[38], assumptions
	efficiency	23 (S2018/20), 30 (S2030) 40 (S2050)	[38], assumptions
GA-plasma-reactor	CO_2 conversion	27 (S2018/20), 35 (S2030) 45 (S2050)	[41], assumptions
	efficiency	43 (S2018/20), 45 (S2030) 50 (S2050)	[41], assumptions
GDE	Current density at 21% oxygen	25 mA/cm^2 (S2018/20) 100 mA/cm^2 (S2030) 200 mA/cm^2 (S2050)	Experimental, assumptions
FTS reactor	CO conversion	50%	PlasmaFuel
Compressors	Isentropic efficiency	80%	PlasmaFuel
Turbines	Isentropic efficiency	80%	PlasmaFuel
Pumps	Isentropic efficiency	80%	PlasmaFuel

Other important technical boundary conditions related to the recycle streams. The parameters regarding recycle streams were chosen the same in all scenarios. A mass fraction of 0.9 was selected for the return of the residual gas to the FTS. For the return after the GDE back to the plasma reactor inlet, a mass fraction of 0.5 was selected.

In addition to the technical parameters, economic boundary conditions must also be set. Table 4 shows cost functions applied in the model and factors used for adjustment via *CEPCI* and for calculating fixed costs. For this purpose, a factor $F_{FCI} = FCI/EC$ was defined, which was calculated from the factors F_j. The factors were selected based on Peters et al. and Albrecht et al. and adjusted for the plasma reactors, electrolysis, and GDE [12,47]. This adjustment was carried out within the framework of the accompanying study BEniVer and applied in the joint project PlasmaFuel.

Table 4. Cost functions and cost factors for calculating the fixed capital investments (FCI) of each component.

Component [Cost Unit]	Cost Function *CF* [Input Unit] [Reference]	*CEPCI* Factor [Year]	F_{FCI} Factor [Reference]
DBD reactor [Mio EUR]	$0.05614 \cdot P_{DBD}[\mathrm{kW}]^{0.5331}$ own assumption, [48]	601.3/607.5 [2019]	1.85 [47], modified
GA reactor [Mio EUR]	$0.1123 \cdot P_{GA}[\mathrm{kW}]^{0.5331}$ own assumption, [48]	601.3/607.5 [2019]	1.85 [47], modified
GDE system [EUR]	$4778 \cdot A_{GDE}\left[\mathrm{m}^2\right]$ own assumption, [6]	601.3/607.5 [2019]	1.44 [47], modified
Electrolysis [EUR]	$793 \cdot P_{EL}$ [kW] [6]	601.3/601.3 [2018]	1.44 [47], modified
FTS reactor [Mio EUR]	$19.8 \cdot \left(\dot{m}_{FTS}\left[\frac{\mathrm{kg}}{\mathrm{s}}\right]/42.2\right)^{0.67}$ [49]	601.3/550.8 [2010]	4.5 [47] modified
Compressor/turbine [EUR]	$2569 \cdot P_C^{0.6782}[\mathrm{kW}]$ [47]	601.3/395.6 [2002]	5 [47]
Pump [EUR]	$14,227 \cdot V_p^{0.3614}\left[\frac{\mathrm{m}^3}{\mathrm{s}}\right]$ [47]	601.3/395.6 [2002]	5 [47]
Heat exchanger [EUR]	$3261 + 170.4 \cdot A_{HEX}\left[\mathrm{m}^2\right]$ [47]	601.3/395.6 [2002]	5 [47]
Reactor/Burner [EUR]	$166.23 \cdot Q_R^{0.8676}[\mathrm{kW}]$ [47]	601.3/395.6 [2002]	5 [47]

In addition to the Factors shown in the Table, material and pressure factors were considered for a few of the components. For pumps and compressors, a material factor of 2.4 for stainless steel was applied; for heat exchangers in the high-pressure section, a pressure factor of 1.16 was applied; and for a turbine located at the purge expansion, a material factor of 5.1 for Ni-coating was applied. The cost functions chosen for the plasma reactors (DBD and GA) should only apply to system sizes of 3 MW and above. Below this limit, we assumed the EUR/kW value of 3 MW, which was EUR 1.300/kW for DBD. This coincided well with the cost of a reactor calculated by Lamberts et al. [34].

To create a cost function ($CF = f(P, ...)$) for the plasma reactors, NREL's 2019 publication of manufacturing costs for PEM electrolyzers was used [50]. Since the reactor systems must first be manufactured, costs for the equipment needed for this were included. The costs of the PEM-EL systems considered there were not only composed of direct and indirect costs. The model used in the publication considered:

The diagram in accordance with the study, shown in Figure 8, reflects how the capital costs for the production facilities and ancillary costs for buildings, labor, etc., decreased when increasing the produced system power. Furthermore, as system power increased, material costs and balance of the plant (BOP) costs also decreased. The data were used to estimate DBD and GA reactor cost functions. Since there was no water cycle involved in the plasma reactors, this part of the BOP was omitted. In addition, cooling cycles were

modeled and simulated separately in the model, so these costs were also omitted. Since the considered GA-plasma reactor was made of other materials due to a higher temperature level, the material costs in the cost function were increased from EUR 200 to EUR 400.

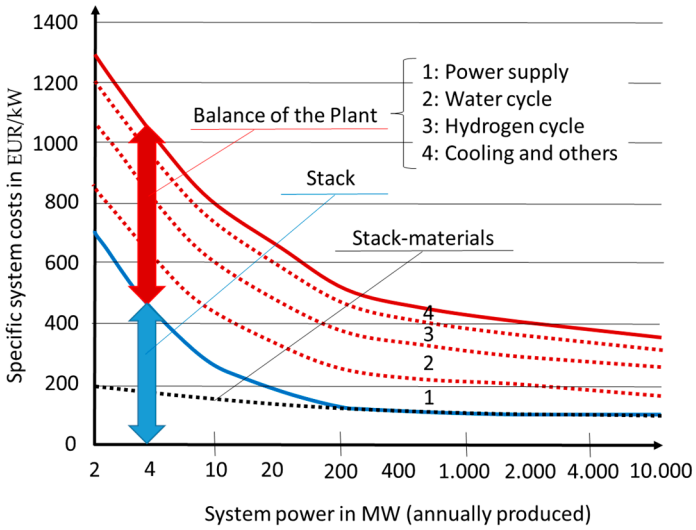

Figure 8. Specific manufacturing costs over system-power of PEM electrolysis systems in accordance with the study of the NREL in 2019 [50].

The GDE cost function assumptions result from calculations with alkaline electrolysis parameters, voltage, and current density, in combination with specific electrolysis system costs [6].

To calculate the direct $OPEX$, the specific costs are listed in Table 5. The specific cost of CO_2 arises from the use of a carbon capture system to clean exhaust gas from a cement plant [50]. The initially assumed electricity costs resulted from averaged market prices from 2018. Later, these costs were again varied based on studies that formulated outlook.

Table 5. Specific costs of expenses and revenues for OPEX calculations.

Expense/Revenue	Specific Cost	Reference
Carbon dioxide (CO_2)	EUR 63/t	[50]
Oxygen (O_2)	EUR 30/t	[34]
Water (H_2O)	EUR 1/t	BEniVer
Cooling water	EUR 0.004/m^3	BEniVer
Waste water	EUR 3.8/m^3	BEniVer
Steam	EUR 16.17/t	BEniVer
electricity	EUR 50/MWh	[51]

In Table 6, factors are listed thatwere used for the calculation of the indirect $OPEX$. For the methodology, the study by Albrecht et al. and the book on plant design and economics were used [12,47]. The indirect $OPEX$ was then calculated according to

$$OPEX, ind = \sum_{k=1}^{8} OPEX, ind, k \quad (18)$$

from the sum of the individual quantities.

Table 6. Factors for calculation of indirect OPEX.

Factor $F_{OPEX,ind}$	Reference Value	Value
$F_{OPEX,ind,1}$	ALC	0.15
$F_{OPEX,ind,2}$	FCI	0.1
$F_{OPEX,ind,3}$	FCI	0.1
$F_{OPEX,ind,4}$	$\sum_{k=2}^{3} OPEX, ind, k$	0.15
$F_{OPEX,ind,5}$	ALC	0.2
$F_{OPEX,ind,6}$	$ALC + \sum_{k=1}^{2} OPEX, ind, k$	0.6
$F_{OPEX,ind,7}$	$OPEX, ind, 6$	0.25
$F_{OPEX,ind,8}$	FCI	0.02

4. Results

This chapter includes the results of the techno-economic analysis. First, the results for the scenarios, defined by the varying parameters, are presented. Shown values are the process efficiency, including the produced amount of fuel and capital costs, as well as the net production costs (NPC) resulting from calculations mentioned in the methodology. Subsequently, several results of the sensitivity analyses are shown.

4.1. Scenarios

The defined scenarios investigated in the analysis differ in the technical parameters of the plasma reactors (conversion and efficiency) and electrolysis (efficiency). Table 7 contains the resulting process efficiencies of the individual scenarios based on the annual product (marine diesel) produced. The projected improvement in component efficiency and conversion increases the amount of product produced by the plant across the scenarios.

Table 7. Process efficiencies of the different scenarios for dielectric barrier discharge (DBD) and gliding Arc (GA) plant.

Plant	Scenario	Process Efficiency in %	Product in (t/Year)
DBD plasma	2018/20	16.5	32,000
	2030	19.6	39,000
	2050	24.4	48,000
GA plasma	2018/20	22.7	45,000
	2030	24.6	49,000
	2050	27.5	54,000

As mentioned in the introduction, a container ship requires a certain amount of energy for typical long-distance transports. Using a lower heating value of $LHV = 43 \frac{\mathrm{MJ}}{\mathrm{kg}}$, a fuel mass of 233 tons of marine diesel is required for each ship. Thus, the 300 MW large-scale plant considered in the scenarios can supply over 200 ships/transport route.

In relation to the above-mentioned technical results of the simulation, the cost of capital for the dielectric barrier discharge (DBD)-plant is shown in Table 8.

A $CAPEX$ of over 1 billion emerge from the modeling of scenario 2018/20. This results, to a large extent, from the oxygen separation via the GDE. Based on the current density curve used in the scenario, an area of $A_{GDE} \approx 142{,}000\ \mathrm{m}^2$ is required. By optimizing the current density curve, a significant decrease in costs can be observed in the scenarios 2030 and 2050. The FTS reactor also requires comparatively high capital costs because, as mentioned in the methodology, a high rate of recycle stream is applied. Due to the increased product yield, these $CAPEX$ increases are negligible.

In the diagrams shown in Figure 9, the net production costs (NPC) of scenario 2018/20 of the DBD plant are broken down. It is clearly visible that both the electricity costs and the $CAPEX$ of the GDE make up a significant share of the costs. The data of the GA-plant, as well as the NPC of the scenarios 2030 and 2050 for each plant, are presented in Figure 10.

Table 8. CAPEX of the different scenarios S2018/20, S2030, and S2050 (DBD-Plant) consisting of investments for the gas diffusion electrode (GDE), dielectric barrier discharge plasma reactor (DBD), electrolysis system (EL), Fischer–Tropsch synthesis reactor (FTS), and other components, e.g., compressors (Comp) and heat exchangers (HEX).

CAPEX in Mio EUR	S2018/20	S2030	S2050
∑	**1350**	**650**	**560**
GDE	970	350	230
DBD	70	50	60
EL	80	60	70
FTS	150	100	100
Others (e.g., Comp, HEX)	80	90	100

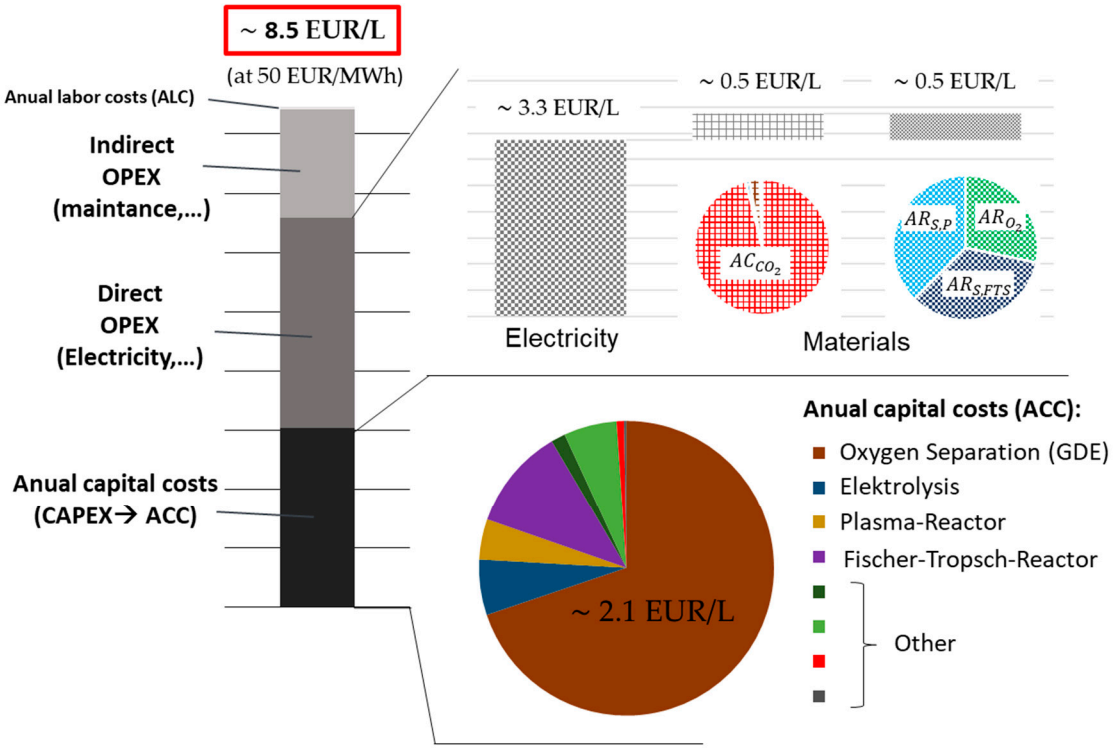

Figure 9. Distribution of net production costs (NPC) of scenario 2018/20 by dielectric barrier discharge (DBD)-plant.

Due to higher capital costs, the part of NPC_{ACC} increases in the case of the gliding arc discharge (GA)-plant. However, since we receive more process heat and can use it to generate steam, which is sold as revenue, $NPC_{OPEXdir}$ decreases by about the same amount as NPC_{ACC} increases.

4.2. Sensitivity Analysis

In addition to the parameter variations within the scope of the scenarios shown, the parameters were varied around the scenario parameters to see the influence on the techno-economic results. Special focus is set on the component parameters of the plasma process. In addition, it is to be found out how large the influence of the GDE is. In the scenarios, a significant reduction in area and thus costs can already be observed by optimizing the characteristic maps.

In the cases shown in Figure 11, some parameters of the plasma reactor and electrolysis are varied around the scenario values. The percentage deviations of the NPC and the process efficiency $\eta_{process}$ from the scenario value are shown. It can be clearly seen that

at low scenario values, i.e., at the plasma-specific values, an increase or decrease has a significantly greater influence on the result. From the percentage deviations of *NPC* and process efficiency shown in the figure, it is evident that the variation of plasma conversion and efficiency by the values chosen in the scenarios exert significant influence. In contrast, further optimization of electrolysis does not result in a large change.

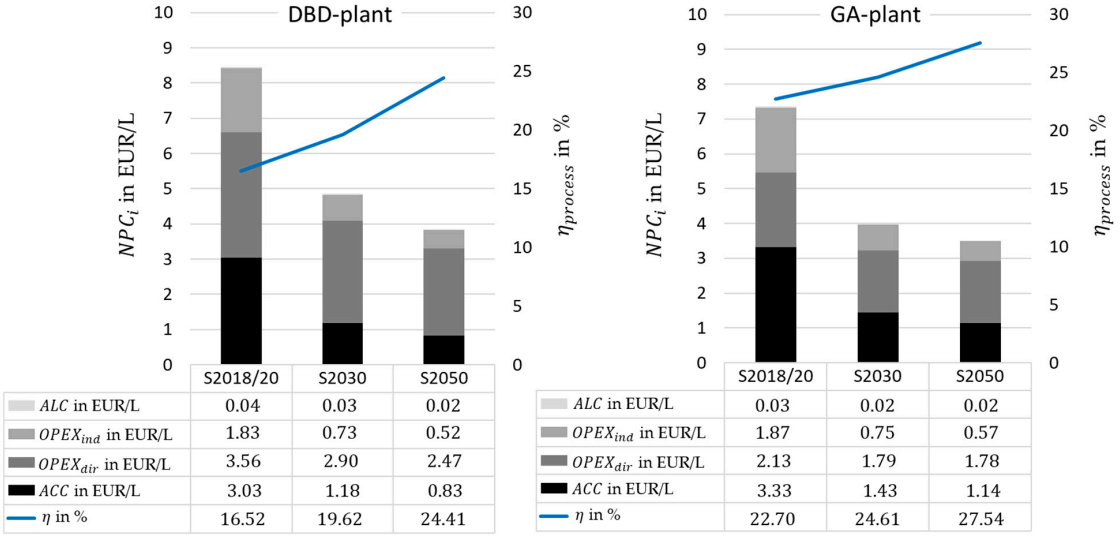

Figure 10. Net production costs (NPC) of scenarios for dielectric barrier discharge (DBD)-plant and gliding arc (GA)-plant.

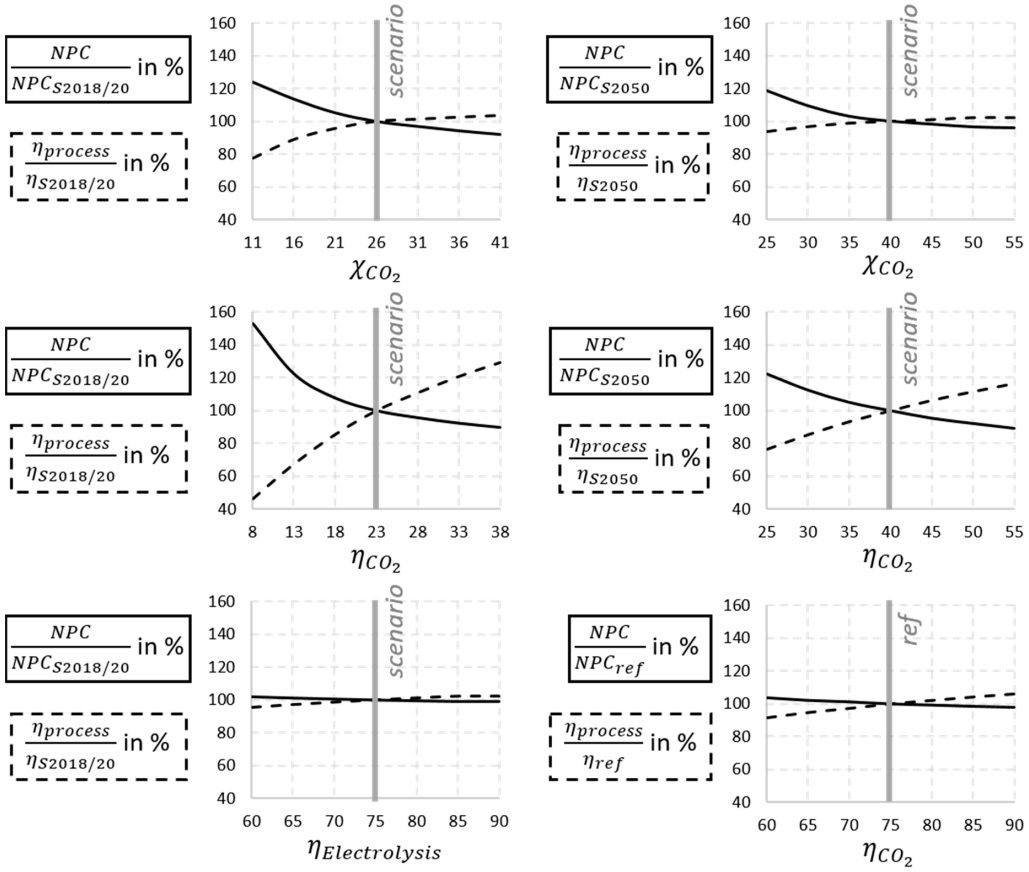

Figure 11. Sensitivity analysis of the plasma reactor and electrolysis parameter. The dotted line describes the process efficiency, the solid line the net production costs (*NPC*).

Figure 12 shows the power distribution among plasma generation, electrolysis, GDE, and all other components, such as compressors and pumps. The power ratio $\left(P_{Plasma} + P_{Electrolysis}\right)/P_{tot}$ decreases significantly with higher efficiencies in syngas generation. It results from more gases being transported by the GDE and the compressors, etc. This can be used to justify the decreasing slope of the process efficiency at higher component efficiencies. As a conclusion from this observation, it can be found that for high-efficiency electrolysis and plasma processes, holistic optimization is necessary. Better compressor efficiencies and more energy-efficient GDE must be investigated to get the maximum potential out of the process.

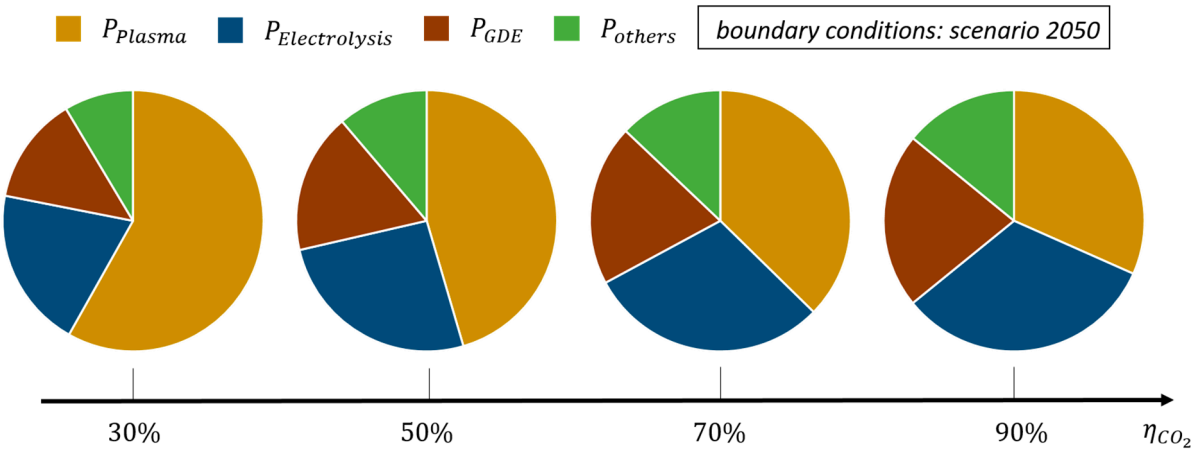

Figure 12. Development of power distribution by increasing the energy efficiency of the plasma-based CO_2 splitting (300 MW total).

The process can also be optimized by adjusting FTS parameters. By changing the process by adjusting temperature and catalysts, the chain growth probability can be influenced. If higher values can be achieved there, the product yield increases significantly. However, product preparation becomes more difficult due to the higher proportion of waxes.

Another optimization option is to increase the CO turnover of the FTS. If this is increased by 5% in the different scenarios, the *NPC* will decrease by EUR 0.2/L at S2018/20 and by EUR 0.1/L at S2050. However, the increase in revenue allows the high recycling rate around the FTS reactor to be eliminated. This also reduces the energy cost of compressing residual gas and the capital cost.

As part of the sensitivity analysis, the characteristic maps of the GDE were also varied. If the optimized GDE current densities of S2050 ($i\left(x_{O_2} = 21\%\right) = 200\ \mathrm{mA/cm^2}$) are already used in the 2018/20 scenario, the *NPC*s decrease from EUR 8.5/L to EUR 5.5/L. This results from a decrease in GDE *CAPEX* from >900 Mio EUR to <200 Mio EUR. On the other hand, if in the 2050 scenario the GDE performance is not optimized as assumed and is according to the performance of S2018/20, the NPC increase from EUR 3.8/L to EUR 6.8/L, resulting from an increase of the GDE *CAPEX* from 200 Mio EUR to 1300 Mio EUR.

The recycle streams were also varied. In Table 9, the main parts of the *NPC* as well as the process efficiency of scenarios 2018/20 and 2050 are shown without the use of recycle streams. The *NPC* are 1.7 times bigger than the scenario values with recycle streams.

Table 9. Results (net production costs *NPC* and process efficiency) using no recycle streams.

	S2018/20 without Recycle	**S2050 without Recycle**
NPC_{ACC} in EUR/L	5.04	1.08
$NPC_{OPEX,dir}$ in EUR /L	6.53	4.70
$NPC_{OPEX,ind}$ in EUR /L	3.03	0.68
NPC_{ALC} in EUR /L	0.05	0.04
NPC in EUR /L	**14.65**	**6.50**
$\eta_{process}$	11%	16.4%

The reduced yield decreases the process efficiency and increases the costs significantly. This results mainly from the recirculation around the FTS reactor, which is why a rate of 0.9 was also chosen in all scenarios. Recirculation around the plasma increases the absolute conversion of CO_2 to CO, but the capital costs increase significantly. Since CO_2 behaves inertly in the FTS reactor, the present ratio between CO_2 and CO has no major influence.

In further sensitivity analyses, different plant sizes were compared. In Figure 13, for scenario 2018/30 and scenario 2050, the parts of the NPC are shown for a 300 MW and a 3 MW plant. It is obvious that the NPC_{ACC} are rising because of the used cost functions and the lost of economy of scale.

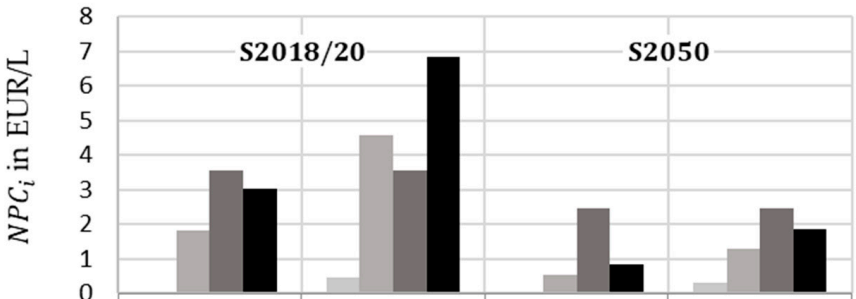

	P_{tot} = 300 MW	P_{tot} = 3 MW	P_{tot} = 300 MW	P_{tot} = 3 MW
NPC_{ALC}	0.04 EUR/L	0.47 EUR/L	0.02 EUR/L	0.32 EUR/L
$NPC_{OPEX,ind}$	1.83 EUR/L	4.58 EUR/L	0.52 EUR/L	1.30 EUR/L
$NPC_{OPEX,dir}$	3.56 EUR/L	3.56 EUR/L	2.47 EUR/L	2.47 EUR/L
NPC_{ACC}	3.03 EUR/L	6.82 EUR/L	0.83 EUR/L	1.87 EUR/L
NPC	8.46 EUR/L	15.43 EUR/L	3.84 EUR/L	5.96 EUR/L

Figure 13. Comparison of net production costs (NPC) of different plant sizes for S2018/20 and S2050.

Based on the hourly share of renewable energy and the corresponding average price per MWh in the European Union, a correlation between these factors could be identified [45]. A high share of renewable energy sources, such as wind and PV, reduces the cost of electrical energy significantly. In the study of ICCT from the year 2020, different scenarios for electricity prices from renewable energies in future were defined [52]. They differ in terms of the generation and transmission of energy. The scenario in which just the generation is observed, so that the user is directly connected to the renewable energy plant, results in electricity costs of c_e = EUR 25/kWh. Because of the flexible operating of plasma-based processes, the reactors could fit with these scenarios. The BEniVer also conducted research and defined scenarios with different electricity prices. The values are shown in Table 10. All mentioned electricity costs are marked in the diagrams shown in Figure 14. Due to the higher process efficiency, the gradients in the diagram for the GA plant are significantly lower.

Table 10. Specific electricity cost minimum and maximum values for the different scenarios, set by BEniVer.

	Minimum Value $c_{e,min}$	**Maximum Value $c_{e,max}$**
S2018/20	EUR 55.7/MWh	EUR 86.6/MWh
S2030	EUR 66.3/MWh	EUR 106.7/MWh
S2050	EUR 40.9/MWh	EUR 81.3/MWh

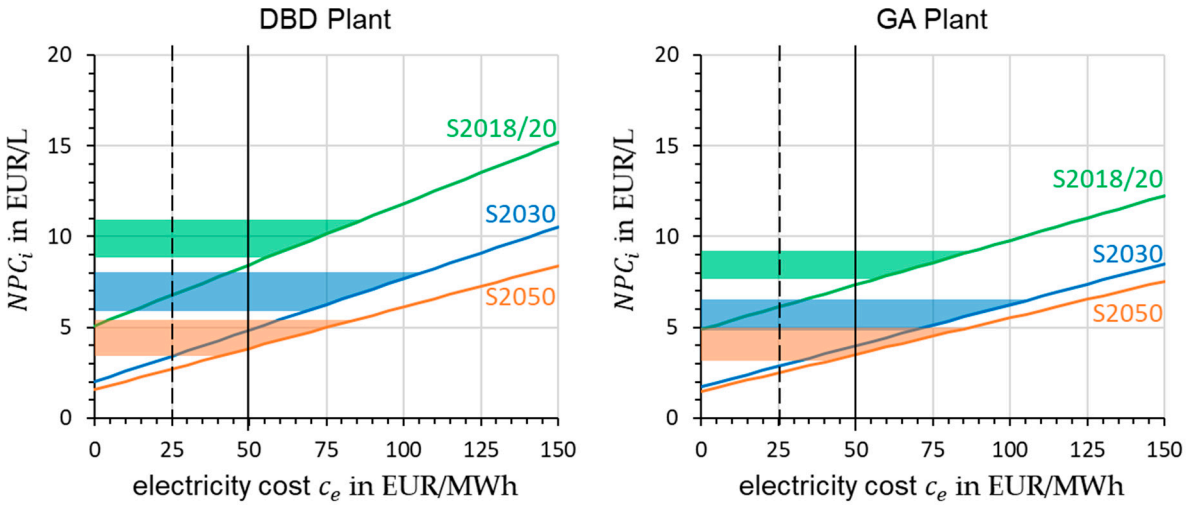

Figure 14. Net production costs (NPC) by varying the electricity cost. The solid vertical line shows the assumption made in the results of the scenarios. The dotted vertical line that of the ICCT scenario described in the text.

5. Discussion—Techno-Economic Potential

The results of the individual scenarios show that the plasma-based CO_2 splitting does not quite reach the values of the Concawe study on the PTL plants with RWGS. In order to get an overview of which combinations of efficiency and conversions go into which cost areas of NPC, the diagrams shown in Figures 15 and 16 were created. The figure shows the NPC over the conversion χ_{CO_2} as well as the efficiency η_{CO_2} of plasma-based CO_2 splitting. For the diagram in Figure 15, other boundary conditions are taken from the 2050 scenario that are important for the overall efficiency are, e.g., $\eta_{EL} = 90\%$ and a higher-performing GDE in terms of current density.

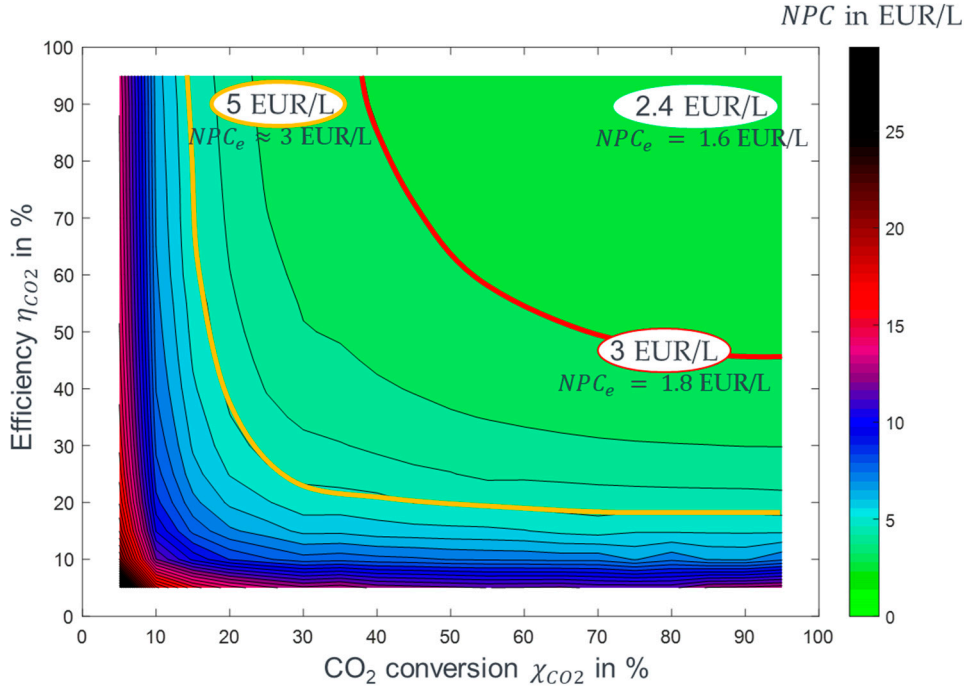

Figure 15. Net production costs (NPC) as a function of CO_2 conversion and energy efficiency; $\eta_{EL} = 90\%$, high-performing GDE.

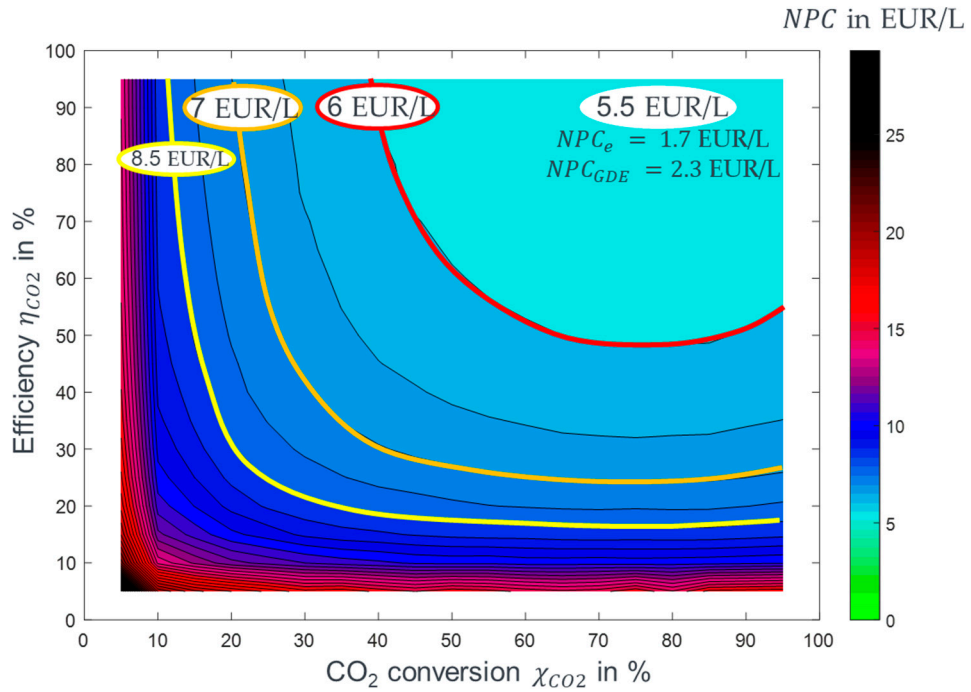

Figure 16. Net production costs (NPC) as a function of CO_2 conversion and energy efficiency; $\eta_{EL} = 75\%$, bad-performing GDE.

At low values of both η_{CO_2} and χ_{CO_2}, unilateral optimization does not have a large impact on the overall performance and, thus, on the NPC. Until the line highlighted in orange at EUR 5/L, there is a high slope of the cost development. This limit can be undercut when reaching $\eta_{CO_2} = \chi_{CO_2} = 25\%$. To reach the value of the fuel costs determined in the Concawe study, conversions and efficiencies must be developed to a level above the red line shown [10]. To get below this cost, efficiencies of at least 45% and revenues of at least 40% must be achieved. By optimizing the GDE and using more efficient compressors and pumps, the efficiency can theoretically be further increased and, thus, $NPC <$ EUR 2.4/L can also be achieved. If the efficiencies of the compressors, turbines, and pumps increase from 80% to 85%, the process efficiency increases by $\Delta\eta_{process} = 0.1\%$, which enables an NPC minimum of EUR 2.2/L. Further cost savings are only feasible through more energy-efficient oxygen separation.

As already shown in the sensitivity analysis, a larger plant capacity leads to a decrease in fuel costs. The PTL plant considered in the Concawe study delivers 1 million tons of product per year (here considered case: <50,000 t), based on the boundary conditions mentioned in the appendix, which leads to the conclusion that the input capacity is significantly larger. As a result, further NPC decreases can be expected if the dimensions are adjusted.

With the supposed development potential of the DBD reactor of $\chi_{CO_2} = \eta_{CO_2} = 40\%$, we get between the two lines shown, thus, a value of EUR 3.8/L can be reached with assumed boundary conditions and electricity costs. For the GA reactor, we suppose a development potential to $\chi_{CO_2} = 45\%$ and $\eta_{CO_2} = 50\%$, thus coming closer to the red line with $NPC =$ EUR 3.5/L. Both reactors reach an equal range of NPC under the scenario assumptions made. Looking at the current state of the research, the values are more in favor of using GA plasma in CO_2-only splitting, as all high-performing DBD reactors do not get above the orange line. The additional capital costs that arise are not considered or offset as in the scenarios via better heat utilization. If other boundary conditions are set to those of scenario 2018/20, the result shown in Figure 16 is achieved. Thus, it is assumed that the electrolysis, as well as the GDE, do not receive any further development.

The minimum $NPC =$ EUR 5.5/L can be seen in the figure as a worst case. Considering the change in power distribution to the main processes plasma and electrolysis and

to auxiliary units GDE as well as peripheral elements such as compressors, etc., shown in the sensitivity analysis, it makes sense to look for alternatives to GDE that do not require electrical energy. If a co-reactant is used in the plasma reactors, O_2 can be avoided as a product. One possibility is to convert CO_2 via dry reforming of methane (DRM), in which CO and H_2 are the products. DRM has already been considered in many papers. In further model variations, the process of a PlasmaFuel follow-up project that will start soon is compared with the predecessor process.

Considering the electricity price from 2018 in Germany, from which the initial assumption of c_e = EUR 50/MWh was made, the operating time can also be adjusted to times with lower costs. This would result in obtaining favorable excess electricity and saving operating costs. In the example year, there are approximately 2000 h at an electricity price below EUR 30/MWh. If the prices are averaged, one gets prices of $c_{e,new} \approx$ EUR 20/MWh, which reduces operating costs by 60%. However, with a reduced operating time, the share of capital costs is also increased. By reducing the operating time by a factor of 4, the NPC_{ACC} share increases by this factor. Applying these two changes to the 2018/20 and 2050 scenarios, we obtain a change in NPC from EUR 8.5/L to EUR 15.4/L for S2018/20 and EUR 3.8/L to EUR 4.8/L for S2050.

6. Conclusions

In the present work, a PTL plant with plasma-based CO_2 splitting was modeled and techno-economically evaluated. Two different technology types, the dielectric barrier discharge plasma (DBD) and the gliding arc discharge plasma (GA), were modeled in different scenarios.

With a defined plant capacity of $P_{tot} = 300$ MW, which is largely distributed between the plasma reactor and electrolysis components, the process efficiencies for the individual scenarios range from $\eta_{process} = 16.5\%$ for scenario 2018/20 to $\eta_{process} = 24.4\%$ for scenario 2050 for the DBD plant. For the GA plant, the process efficiency ranges from 22.7% to 27.5%. The differences between the individual scenarios are based on improved characteristic values of individual components as well as on changed parameters used in the calculations. The total capital investment $CAPEX$ in the considered process is estimated at 1350 Mio EUR or scenario 2018/20, 650 Mio EUR for scenario 2030, and 560 Mio EUR for scenario 2050. The main cost driver is the gas diffusion electrode (GDE) for oxygen separation, which accounts for between 30% (2050 scenario) and 70% (2018/20 scenario) of the $CAPEX$. Including all annual costs, the net production cost (NPC) for the generated product ranges from NPC = EUR 8.5/L for scenario 2018 to NPC = EUR 3.8/L for scenario 2050 for the DBD plasma plant and EUR 7.3/L to EUR 3.5/L for the GA plasma plant.

From sensitivity analyses to the scenarios, dependencies of $\eta_{process}$ and NPC to variations of technical sizes are considered. Especially the conversion rate and energy efficiency of the plasma reactor have a great impact on the results due to relatively low values. Reaching higher performance, the influence of value increase has a lower impact because of the power requirements of supporting components like the GDE or compressors. Downscaling the modeled process to $P_{tot} = 3$ MW, without adjusting other parameters, increases costs by ΔNPC = EUR 7/L for scenario 2018/20 and by ΔNPC = EUR 2.1/L for scenario 2050. The reason for this is non-linearly scaling equipment costs. If cheaper electricity is used, as assumed, for example, in a study by the ICCT for 2050 with a direct connection to a renewable energy system such as photovoltaics, a fuel price of approx. EUR 2/L can be achieved in the scenarios examined.

At low values of both η_{CO_2} and χ_{CO_2}, unilateral optimization does not have a large impact on the overall performance and, thus, on the NPC. Until EUR 5/L, there is a high slope of cost development. This limit can be undercut when reaching $\eta_{CO_2} = \chi_{CO_2} = 25\%$. To get below EUR 3/L cost, efficiencies of at least 45% and revenues of at least 40% must be achieved. By optimizing the GDE and using more efficient compressors and pumps, the efficiency can theoretically be further increased and, thus, $NPC <$ EUR 2.4/L can also be achieved.

The present work provides an extension to previous studies on the techno-economics of PtL processes. By looking at the scenarios, it is moreover possible to distinguish between the different development levels of plasma and GDE technology. The sensitivity analysis illustrates the significant influence of component optimization on existing values. The techno-economic potential, shown in Figure 15, highlights the benchmarks of conversion and efficiency. In addition, the processing by gas separation is emphasized, which in this work is carried out by the GDE and is currently very energy- and cost-intensive. The variations made, and the mapping of the potential furthermore provide an extension to economic studies like the work of Lamberts et al., in which the economics of a DBD plasma reactor is investigated. The results of the present study reflect the direction of further development of plasma-based CO_2 splitting for use in PtL plants. The relatively low conversion rates of plasma reactors, in contrast to electrolysis, can be counteracted to a certain extent using recycle streams. However, the crucial point for the classification of the process in the PtL sector lies in the characteristic values of the GDE. The low costs in the 2030 and 2050 scenarios result, to a large extent, from the reduction of the GDE costs by improving the current density. Therefore, the further development of this characteristic value is decisive for the use of plasma-induced CO_2 splitting in the PtL process. If this is successful, plasma-based CO_2 splitting can be a viable alternative to RWGS CO_2 splitting due to its scalability, flexibility, and process without external thermal heat supply via a burner.

Author Contributions: Writing: S.J.K. and P.R.; experimental: S.R., M.L. and J.S.; modeling and techno-economic analysis: S.J.K. and M.R.; text review: V.S.; supervision: K.P.B. All authors have read and agreed to the published version of the manuscript.

Funding: This research was part of the PlasmaFuel joint project, which was funded by Bundesministerium für Wirtschaft und Klimaschutz (BMWK) with grant number 03EIV161A-D.

Institutional Review Board Statement: Not applicable.

Informed Consent Statement: Not applicable.

Data Availability Statement: Research data can be provided upon request.

Acknowledgments: The authors would like to thank the partners of the PlasmaFuel project as well as the BEniVer accompanying study of the DLR for their support in learning the topic of techno-economic analysis. A big thank you also to the university, the institute, and friends and family for their daily support.

Conflicts of Interest: The authors declare no conflict of interest.

Appendix A

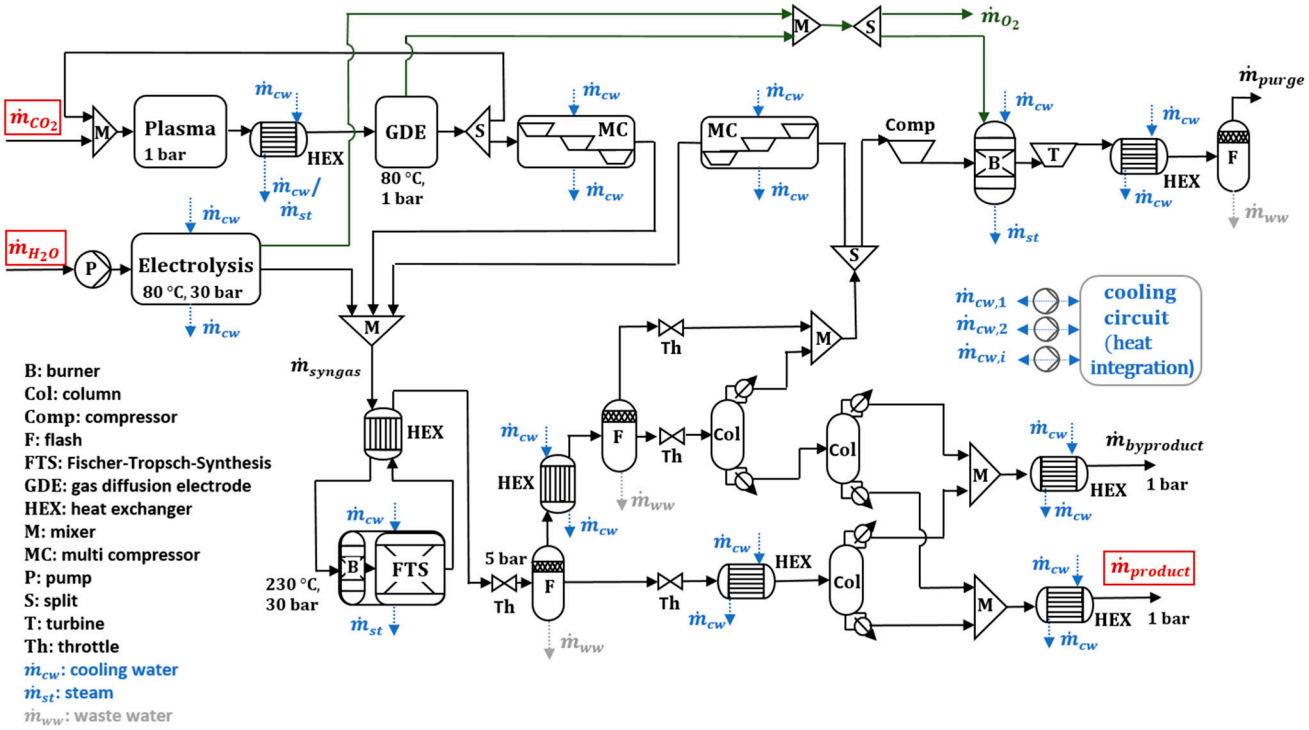

Figure A1. Flowsheet.

References

1. Olivier, J.G.J.; Peters, J.A.H.W. Trends in Global CO_2 and Total Greenhouse Gas Emissions: 2020 Report. 2020. Available online: http://www.pbl.nl/en (accessed on 8 February 2023).
2. International Energy Agency. International Energy Agency (IEA) World Energy Outlook 2022. 2022, p. 524. Available online: https://www.iea.org/reports/world-energy-outlook-2022 (accessed on 8 February 2023).
3. Eurostat Renewable Energy Statistics. Available online: https://ec.europa.eu/eurostat/statistics-explained/index.php?title=Renewable_energy_statistics#Share_of_renewable_energy_more_than_doubled_between_2004_and_2021 (accessed on 8 February 2023).
4. BMWi and AGEE-Stat. Zeitreihen zur Entwicklung der erneuerbaren Energien in Deutschland (Stand: Februar 2014). 2014. Available online: https://www.erneuerbare-energien.de/EE/Navigation/DE/Service/Erneuerbare_Energien_in_Zahlen/Zeitreihen/zeitreihen.html (accessed on 8 February 2023).
5. Jahr, D.; Zwischenziele, D.; Energien-gesetzes, E.; Eu-gesetzgebung, D.; Ziele, D. *Erneuerbare Energien 2022 Zubauzahlen und beschlossene Beschleunigungsmaßnahmen im Überblick (National + Europäisch)*; Bundesministerium für Wirtschaft und Klimaschutz: Berlin, Germany, 2023; pp. 1–8.
6. Smolinka, T.; Wiebke, N.; Sterchele, P.; Lehner, F.; Jansen, M. *Studie IndWEDe Industrialisierung der Wasserelektrolyse in Deutschland: Chancen und Herausforderungen für Nachhaltigen Wasserstoff für Verkehr, Strom und Wärme*; NOW GmbH: Berlin, Germany, 2018.
7. Maia Research. Global Syngas Market Research Report 2022. 2022, p. 116. Available online: https://www.marketresearch.com/QYResearch-Group-v3531/Global-Piperonal-Research-31676097/ (accessed on 8 February 2023).
8. Finanzen.net. Erdgaspreisentwicklung. Available online: https://www.finanzen.net/rohstoffe/erdgas-preis-natural-gas/chart/euro (accessed on 8 February 2023).
9. Sofia, D.; Giuliano, A.; Poletto, M.; Barletta, D. Techno-economic analysis of power and hydrogen co-production by an IGCC plant with CO_2 capture based on membrane technology. In *Computer Aided Chemical Engineering*; Elsevier: Amsterdam, The Netherlands, 2015; Volume 37, pp. 1373–1378. [CrossRef]
10. Soler, A.; Schmidt, P. E-Fuels: A techno-economic assessment of European domestic production and imports towards 2050. In Proceedings of the 14th Concawe Symposium, Virtual, 27–28 September 2021; pp. 27–28.
11. Giuliano, A.; Catizzone, E.; Freda, C. Process Simulation and Environmental Aspects of Dimethyl Ether Production from Digestate-Derived Syngas. *Int. J. Environ. Res. Public Health* **2021**, *18*, 807. [CrossRef] [PubMed]
12. Albrecht, F.G.; König, D.H.; Baucks, N.; Dietrich, R.-U. A standardized methodology for the techno-economic evaluation of alternative fuels—A case study. *Fuel* **2017**, *194*, 511–526. [CrossRef]

13. Bundesministerium für Wirtschaft und Klimaschutz. *Bareiß: Forschungsinitiative „Energiewende im Verkehr "-150 Förderprojekte gehen an den Start*; Press release; Bundesministerium für Wirtschaft und Klimaschutz: Berlin, Germany, 2019.
14. Verband der Chemischen Industrie. *Ermittlung der Treibhausgas-Emissionen in Transport und Logistik der Chemisch- Pharmazeutischen Industrie*; Verband der Chemischen Industrie: Frankfurt, Germany, 2021.
15. Bogaerts, A.; Tu, X.; Whitehead, J.C.; Centi, G.; Lefferts, L.; Guaitella, O.; Azzolina-Jury, F.; Kim, H.-H.; Murphy, A.B.; Schneider, W.F.; et al. The 2020 plasma catalysis roadmap. *J. Phys. D Appl. Phys.* **2020**, *53*, 443001. [CrossRef]
16. Bogaerts, A.; Centi, G. Plasma Technology for CO_2 Conversion: A Personal Perspective on Prospects and Gaps. *Front. Energy Res.* **2020**, *8*, 111. [CrossRef]
17. North, M.; Abrantes, P.; Remiezowicz, E.; Bardow, A.; Dodson, J.; Manning, T.; Albo, J.; Reed, D.; Harris, D.; Ingram, I.; et al. CO_2 reduction reactions: General discussion. *Faraday Discuss.* **2015**, *183*, 261. [CrossRef]
18. Snoeckx, R.; Bogaerts, A. Plasma technology—A novel solution for CO_2 conversion? *Chem. Soc. Rev.* **2017**, *46*, 5805–5863. [CrossRef] [PubMed]
19. Mehta, P.; Barboun, P.; Go, D.B.; Hicks, J.C.; Schneider, W.F. Catalysis Enabled by Plasma Activation of Strong Chemical Bonds: A Review. *ACS Energy Lett.* **2019**, *4*, 1115–1133. [CrossRef]
20. Puliyalil, H.; Jurković, D.L.; Dasireddy, V.D.B.C.; Likozar, B. A review of plasma-assisted catalytic conversion of gaseous carbon dioxide and methane into value-added platform chemicals and fuels. *RSC Adv.* **2018**, *8*, 27481–27508. [CrossRef]
21. Van Durme, J.; Dewulf, J.; Leys, C.; Van Langenhove, H. Combining non-thermal plasma with heterogeneous catalysis in waste gas treatment: A review. *Appl. Catal. B Environ.* **2008**, *78*, 324–333. [CrossRef]
22. Mizuno, A. Industrial applications of atmospheric non-thermal plasma in environmental remediation. *Plasma Phys. Control. Fusion* **2007**, *49*, A1–A15. [CrossRef]
23. Chen, J.G.; Crooks, R.M.; Seefeldt, L.C.; Bren, K.L.; Bullock, R.M.; Darensbourg, M.Y.; Holland, P.L.; Hoffman, B.; Janik, M.J.; Jones, A.K.; et al. Beyond fossil fuel–driven nitrogen transformations. *Science* **2018**, *360*, eaar6611. [CrossRef] [PubMed]
24. Liu, L.; Zhang, Z.; Das, S.; Kawi, S. Reforming of tar from biomass gasification in a hybrid catalysis-plasma system: A review. *Appl. Catal. B Environ.* **2019**, *250*, 250–272. [CrossRef]
25. Du, C.; Mo, J.; Li, H. Renewable Hydrogen Production by Alcohols Reforming Using Plasma and Plasma-Catalytic Technologies: Challenges and Opportunities. *Chem. Rev.* **2014**, *115*, 1503–1542. [CrossRef]
26. Tu, X.; Whitehead, J.C.; Nozaki, T. Plasma Catalysis: Fundamentals and Applications. In *Plasma Catalysis*; Springer: Berlin/Heidelberg, Germany, 2019; Volume 2019. [CrossRef]
27. Renninger, S.; Rößner, P.; Stein, J.; Lambarth, M.; Birke, K.P. Towards High Efficiency CO_2 Utilization by Glow Discharge Plasma. *Processes* **2021**, *9*, 2063. [CrossRef]
28. Trenchev, G.; Bogaerts, A. Dual-vortex plasmatron: A novel plasma source for CO_2 conversion. *J. CO_2 Util.* **2020**, *39*, 101152. [CrossRef]
29. Kim, S.C.; Lim, M.S.; Chun, Y.N. Reduction Characteristics of Carbon Dioxide Using a Plasmatron. *Plasma Chem. Plasma Process.* **2013**, *34*, 125–143. [CrossRef]
30. Kim, H.; Song, S.; Tom, C.P.; Xie, F. Carbon dioxide conversion in an atmospheric pressure microwave plasma reactor: Improving efficiencies by enhancing afterglow quenching. *J. CO_2 Util.* **2019**, *37*, 240–247. [CrossRef]
31. Bongers, W.; Bouwmeester, H.; Wolf, B.; Peeters, F.; Welzel, S.; Bekerom, D.V.D.; Harder, N.D.; Goede, A.; Graswinckel, M.; Groen, P.W.; et al. Plasma-driven dissociation of CO_2 for fuel synthesis. *Plasma Process. Polym.* **2016**, *14*, 1600126. [CrossRef]
32. Snoeckx, R.; Ozkan, A.; Reniers, F.; Bogaerts, A. The Quest for Value-Added Products from Carbon Dioxide and Water in a Dielectric Barrier Discharge: A Chemical Kinetics Study. *Chemsuschem* **2016**, *10*, 409–424. [CrossRef]
33. Uytdenhouwen, Y.; Van Alphen, S.; Michielsen, I.; Meynen, V.; Cool, P.; Bogaerts, A. A packed-bed DBD micro plasma reactor for CO_2 dissociation: Does size matter? *Chem. Eng. J.* **2018**, *348*, 557–568. [CrossRef]
34. Assche, H.L.-V.; Thomassen, G.; Compernolle, T. The early-stage design of plasma for the conversion of CO_2 to chemicals: A prospective techno-economic assessment. *J. CO_2 Util.* **2022**, *64*, 102156. [CrossRef]
35. Spencer, L.F.; Gallimore, A.D. Efficiency of CO_2 Dissociation in a Radio-Frequency Discharge. *Plasma Chem. Plasma Process.* **2010**, *31*, 79–89. [CrossRef]
36. Andreev, S.; Zakharov, V.; Ochkin, V.; Savinov, S. Plasma-chemical CO_2 decomposition in a non-self-sustained discharge with a controlled electronic component of plasma. *Spectrochim. Acta Part A Mol. Biomol. Spectrosc.* **2004**, *60*, 3361–3369. [CrossRef] [PubMed]
37. Raja, B.; Sarathi, R.; Vinu, R. Development of a Swirl-Induced Rotating Glow Discharge Reactor for CO_2 Conversion: Fluid Dynamics and Discharge Dynamics Studies. *Energy Technol.* **2020**, *8*, 2000535. [CrossRef]
38. Ozkan, A.; Bogaerts, A.; Reniers, F. Routes to increase the conversion and the energy efficiency in the splitting of CO_2 by a dielectric barrier discharge. *J. Phys. D Appl. Phys.* **2017**, *50*, 084004. [CrossRef]
39. Uytdenhouwen, Y.; Bal, K.; Neyts, E.; Meynen, V.; Cool, P.; Bogaerts, A. On the kinetics and equilibria of plasma-based dry reforming of methane. *Chem. Eng. J.* **2020**, *405*, 126630. [CrossRef]
40. Renninger, S.; Lambarth, M.; Birke, K.P. High efficiency CO_2-splitting in atmospheric pressure glow discharge. *J. CO_2 Util.* **2020**, *42*, 101322. [CrossRef]
41. Renninger, S.; Stein, J.; Lambarth, M.; Birke, K.P. An optimized reactor for CO_2 splitting in DC atmospheric pressure discharge. *J. CO_2 Util.* **2022**, *58*, 101919. [CrossRef]

42. Renninger, S.; Lambarth, B.J. BMBF Projectreport PlasmaFuel. 2023; Report available upon request.
43. Buck, F.; Kistner, I.; Rösler, C.; Schulz, A.; Walker, M.; Tovar, G.E.M.; Schiestel, T.; Tovar, G. Einsatz von perowskitischen Hohlfasermembranen in einem Mikrowellenplasma. *Chem. Ing. Tech.* **2019**, *91*, 1117–1122. [CrossRef]
44. Perez-Carbajo, J.; Matito-Martos, I.; Balestra, S.R.G.; Tsampas, M.N.; van de Sanden, M.C.M.; Delgado, J.A.; Águeda, V.I.; Merkling, P.J.; Calero, S. Zeolites for CO_2–CO–O_2 Separation to Obtain CO_2-Neutral Fuels. *ACS Appl. Mater. Interfaces* **2018**, *10*, 20512–20520. [CrossRef]
45. IEA. *The Future of Hydrogen*; No. June; OECD: Paris, France, 2019. [CrossRef]
46. Van de Loosdrecht, J.; Botes, F.G.; Ciobica, I.M.; Ferreira, A.C.; Gibson, P.; Moodley, D.J.; Saib, A.M.; Visagie, J.L.; Weststrate, C.J.; Niemantsverdriet, J.W. Fischer–Tropsch Synthesis: Catalysts and Chemistry. *Surf. Inorg. Chem. Heterog. Catal.* **2013**, *7*, 525–557. [CrossRef]
47. Peters, M.S.; Timmerhaus, K.D.; West, R.E. *Plant Design and Economics for Chemical Engineers*; McGraw-Hill: New York, NY, USA, 2003; Volume 4.
48. Mayyas, A.T.; Ruth, M.F.; Pivovar, B.S.; Bender, G.; Wipke, K.B. *Manufacturing Cost Analysis for Proton Exchange Membrane Water Electrolyzers*; Technical Report NREL/TP-6A20-72740; National Renewable Energy Laboratory: Golden, CO, USA, 2019.
49. Hannula, I. Liquid Transportation Fuels via Large-Scale Fluidised-Bed Gasification of Lignocellulosic Biomass. Available online: http://www.vtt.fi/publications/index.jsp (accessed on 8 February 2023).
50. Roussanaly, S.; Fu, C.; Voldsund, M.; Anantharaman, R.; Spinelli, M.; Romano, M. Techno-economic Analysis of MEA CO_2 Capture from a Cement Kiln—Impact of Steam Supply Scenario. *Energy Procedia* **2017**, *114*, 6229–6239. [CrossRef]
51. Bundesnetzagentur. Bundesnetzagentur SMARD Strommarktdaten. Available online: https://www.smard.de/home (accessed on 8 February 2023).
52. Christensen, A. Assessment of Hydrogen Production Costs from Electrolysis: United States and Europe. International Council on Clean Transportation (ICCT). Available online: https://theicct.org/sites/default/files/publications/final_icct2020_assessment_of_hydrogen_production_costsv2.pdf (accessed on 8 February 2023).

Disclaimer/Publisher's Note: The statements, opinions and data contained in all publications are solely those of the individual author(s) and contributor(s) and not of MDPI and/or the editor(s). MDPI and/or the editor(s) disclaim responsibility for any injury to people or property resulting from any ideas, methods, instructions or products referred to in the content.